2021학년도 학생주도
창의연구프로젝트 연구 결과보고서

[연구과제명: 셔틀탱커에 작용하는 2차 파력의 실험적/수치적 연구]

2022. 1.

창원대학교 R&D혁신본부
(R&D지원실)

목 차

2021학년도 학생주도 창의연구프로젝트 연구 중간 보고서

☐ 연구팀명: SDCL Drift

☐ 연구과제명: 셔틀탱커에 작용하는 2차 파력의 실험적/수치적 연구

☐ 참여 연구원 명단

구 분	소 속	직 급	성 명	연구분담내용	비고
책임연구원	스마트환경에너지 공학과정	석사과정	마이반투안	총괄, 보고서작성	
연구원	스마트환경에너지 공학과정	박사과정	응웬티당디엡	모형시험	
연구원	스마트환경에너지 공학과정	석사과정	이산	이론해석	학석사
지도교수 (전임교원)	조선해양공학과	교수	윤현규	자문	

2021년도 「학생주도 창의연구프로젝트 연구」 결과 보고서를 제출합니다.

2022년 1월 28일

연구책임자 소속 : 스마트환경에너지공학과정 직 : 석사과정 성명 : 마이반투안 (인)

창원대학교 총장 귀하

Ⅰ. 학생주도 창의연구프로젝트 결과 보고서

1. 목적 및 필요성

○ 연구의 목적

- Estimate the 2nd-order wave drift force acting on the shuttle tanker in regular waves with various wave directions at zero speed numerically by ANSYS AQWA.
- Estimate the 2nd-order wave drift force depending on various wave directions and wavelength experimentally by model tests in wave tank.
- Compare the experimental results and numerical results, and then suggest 2nd-order wave drift force model for DP simulation.

○ 연구의 필요성

- Analysis of wave effects on the shuttle tanker when shuttle tanker receives oil from offshore to ship or transfers the oil from the ship to onshore refineries is necessary to design it properly even in harsh sea condition.
- Dynamic positioning is necessary for the shuttle tanker to be operated safely, and for this purpose, unpredictable wave drift force is a major influence on the performance of the dynamically positioned ship’ s offloading.

< Shuttle tanker during offloading and DP concept >

2. 연구범위 및 방법

○ 연구 범위

- Estimation of the 2nd-order wave drift force numerically
- Estimation of the 2nd-order wave drift force experimentally
- Comparison of experimental and numerical results and suggestion of the 2nd-order wave drift force model for DP simulation

○ 연구 방법

Estimation of the 2nd-order wave drift force numerically

- Choose calculation conditions (Wave frequencies and directions)
- Adopt and draw the geometry of a shuttle tanker (e.g. KVLCC2)
- Mesh and pre-processing
- Solver and export the result by ANSYS AQWA

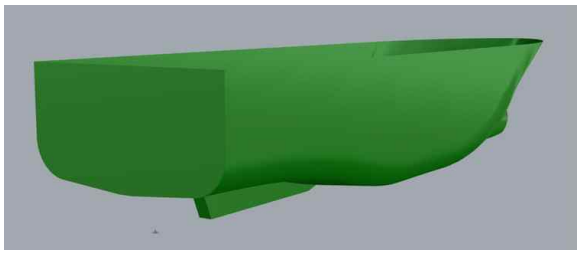

< Geometry of shuttle tanker and meshing >

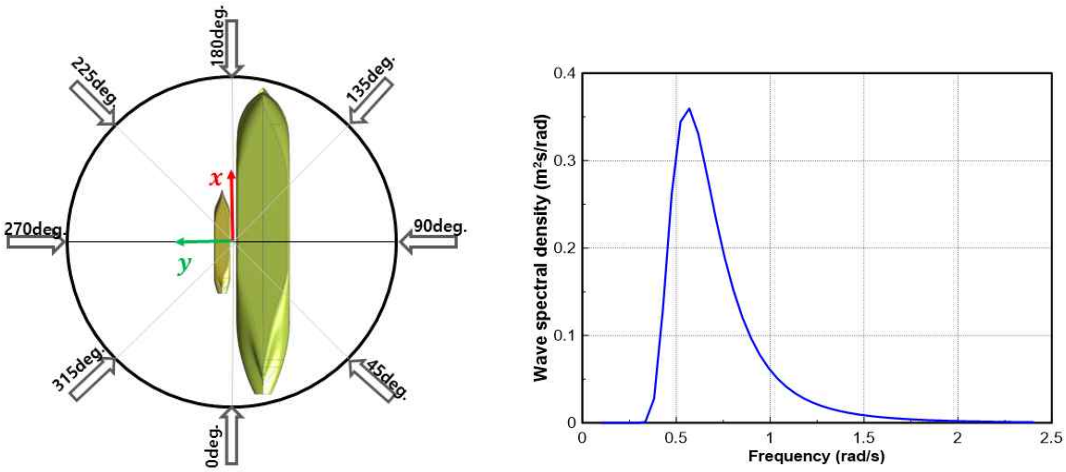

< Wave direction and wave spectrum >

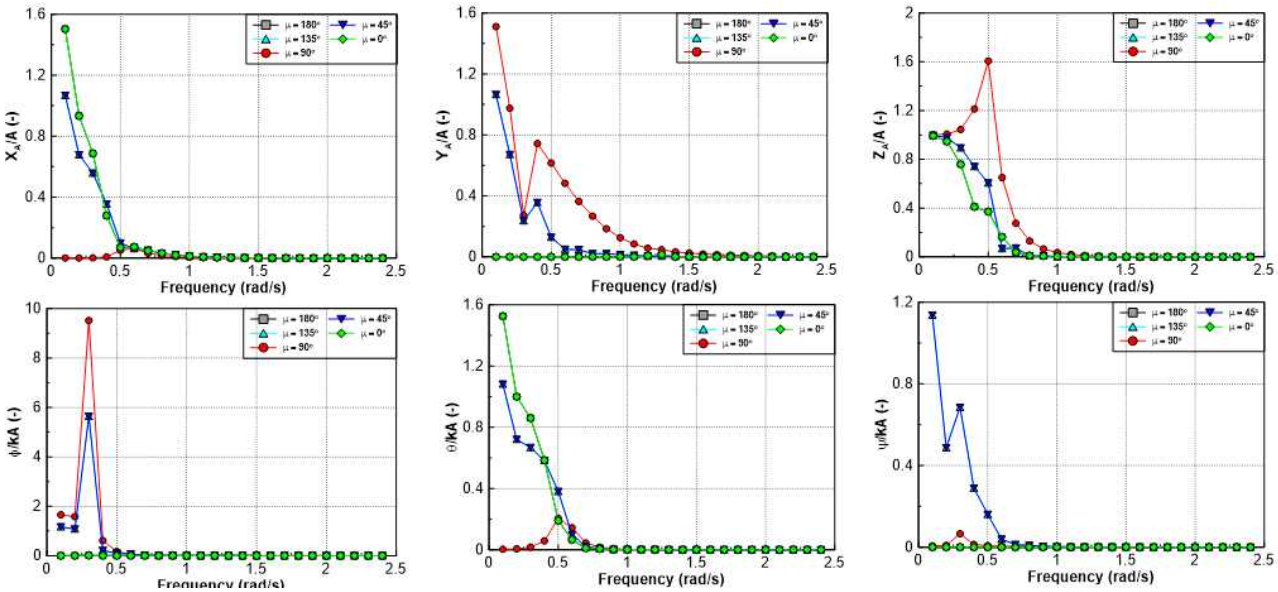

< Sample results of KVLCC2 in various wave directions and frequencies >

Estimation of the 2nd-order wave drift force experimentally

- Make the shuttle tanker with a model scale of about 1/11
  (Stocked model ship - KVLCC2 will be used)
- Generate wave and confirm the wave quality in wave tank
- Experimental setup
- Perform the experiment and data analysis

< Shuttle tanker model >

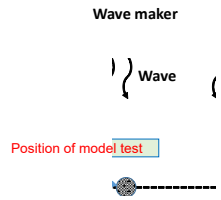

< Generate wave and confirm the wave quality >

< Experimental setup and sample time series of wave drift force >

Comparison of experimental and numerical results and suggestion of the 2nd-order wave drift force model for DP simulation

- Comparison of 2nd-order wave drift force for different wave directions and wave length calculated by ANSYS AQWA and measured by the model test in wave tank
- Suggestion of 2nd-order wave drift force model to simulate dynamic positioning of a shuttle tanker which will be used in HIL(Hardware-In-the-Loop) simulation test of DP simulator

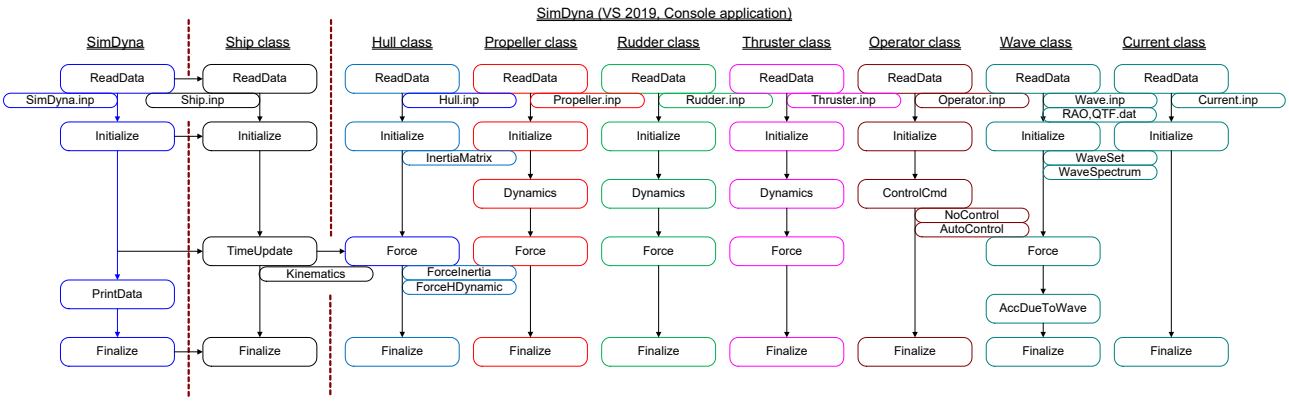

< HIL test class diagram including wave class >

3. 연구수행 내용

1. Introduction

In this study, numerical method and experiment were applied to estimate wave drift force and RAOs (Response Amplitude Operator) of KVLCC2 in waves. The analysis of wave effects on the general sea transportation as well as shuttle tanker separately when shuttle tanker receives oil from offshore to ship or transfers the oil from the ship to onshore refineries is necessary to design it properly even it harsh sea condition. Dynamic positioning is necessary for the shuttle tanker to be operated safely, and for this purpose, unpredictable wave drift force is a major influence on the performance of the dynamically positioned ship's offloading. In numerical method, the estimation of the 2nd-order wave drift forces acting on the KVLCC2 tanker in regular waves with various directions at zero speed numerically was calculated by ANSYS AQWA. The model test are conducted in a rectangular water basin equipped with a wavemaker. The 2nd-order wave drifts force depending on various wave directions and wavelength experimentally by model tests in the wave tank. Through this study, the result of the wave drift forces and RAOs on KVLCC2 were compared from the numerical methods by AQWA with other numerical result of GL Rankin code and experiments results.

2. Description of KVLCC2

The model ship which used in this research for simulation is the KRISO Very Large Crude Carrier 2 (KVLCC2). Fig. 2.1 shows the body plan and side view of the KVLCC2 ship model. Table 2.1 provides the principal particulars of the KVLCC2 model.

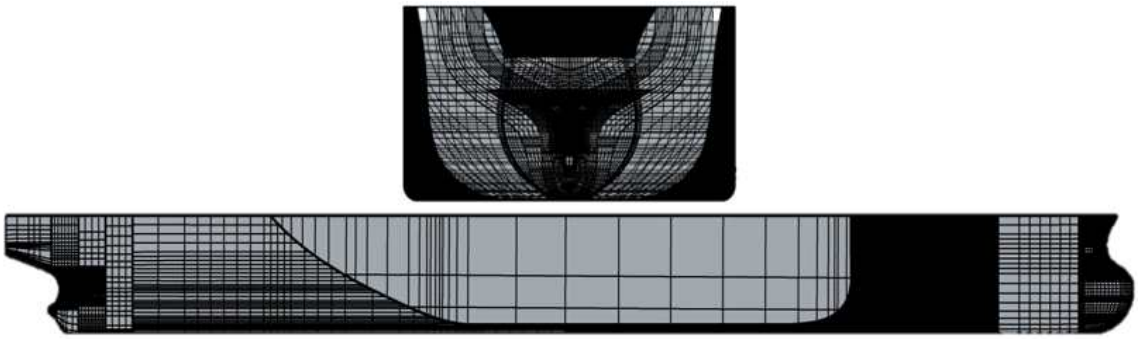

Fig. 2.1 Body plan and side view of the KVLCC2 ship model.

Table 2.1 Main dimensions of KVLCC2

Specification		Unit	Full scale	Model scale
Length between perpendiculars	Lpp	m	320.0	1.435
Length of water line	Lwl	m	325.5	1.460
Maximum beam of water line	Bwl	m	58.0	0.260
Depth	D	m	30.0	0.135
Draft	T	m	20.8	0.093
Displacement volume	▽	kg.f	312622	1401.892
Water plane area	Aw	m^2	27711	0.557
Vertical center of gravity	KG	m	18.6	0.083
Metacentric height	GM	m	5.71	0.026
Moment of Inertia	Kxx/Bwl	-	0.40	0.002
Moment of Inertia	Kyy/Lpp, Kzz/Lpp	-	0.25	0.001

3. Numerical Method

3.1. Coordinate system

Ship motion can represented on a right handed Cartesian coordinate system as shown in fig. 3.1. The displacement of a ship in x, y, z direction are surge, sway, and heave, respectively. Rotational displacement of a ship about the same axis respectively are roll ϕ, pitch θ, and yaw ψ, respectively. The wave direction is defined as shown in Fig. 3.2.

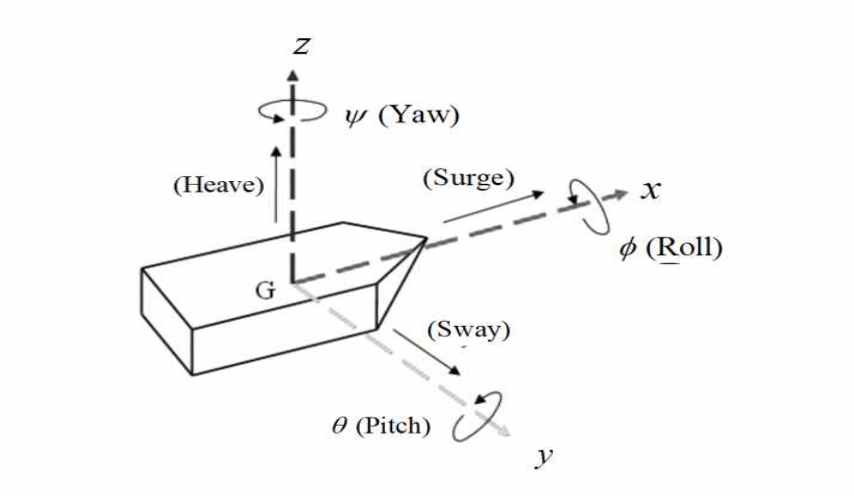

Fig. 3.1 Coordinate system

Fig. 3.2 Wave direction

3.2.Theoretical formulation

3.2.1.Three-dimensional panel method

In this study, the ANSYS AQWA program was used. It is based on the three-dimensional panel method in the frequency domain with the assumption of velocity potential. The ship fixed coordinate system is defined in Fig. 3.2 to solve the ship motion values. According to Newton's second law, Cauchy equation, Navier-Stokes equation, Euler equation, we are obtained the Bernoulli Eq. (3.1)

$$\rho\frac{\partial\Phi}{\partial t}+P+\frac{1}{2}\rho|\nabla\Phi|^2+\rho gZ=C(t) \tag{3.1}$$

The equation (3.2-3.3) are obtained the Laplace equation ∇^2 is the Laplace operator, further the continuity equation is of the form:

$$\nabla^2\Phi=0 \tag{3.2}$$

$$\frac{\partial^2\Phi}{\partial x^2}+\frac{\partial^2\Phi}{\partial y^2}+\frac{\partial^2\Phi}{\partial z^2}=0 \tag{3.3}$$

$$\Phi_T=\Phi_I+\Phi_D+\Phi_R \tag{3.4}$$

Equation (3.4) called velocity potential, (Φ_I) affected the incident wave velocity potential which assumed that the incident wave is not disturbed by the vessel. (Φ_D) Diffraction wave velocity potential the force caused by the wave disturbed by the presence of the vessel with object fixation. (Φ_R) Radiation wave velocity potential, the forces acting due to forced oscillations of ships in time constant. Substitute Laplace equation (3.4) into Bernoulli equation (3.1):

$$P=-\rho gz-\rho\frac{\partial\Phi}{\partial t}=-\rho gz-\rho\left(\frac{\partial\Phi_I}{\partial t}+\frac{\partial\Phi_D}{\partial t}+\frac{\partial\Phi_R}{\partial t}\right) \tag{3.5}$$

The velocity potential representation by superposition and decomposition Eq. (3.6-3.7):

$$\Phi_T = (x, y, z, t) = \Phi_I(x, y, z, t) + \Phi_D(x, y, z, t) + \Phi_R(x, y, x, t) \tag{3.6}$$

$$= \{\Phi_I(x, y, z) + \Phi_D(x, y, z) + \Phi_R(x, y, z)\}e^{i\omega t}$$

$$\Phi_T(x, y, z) = \Phi_I(x, y, z) + \Phi(LSUBDx, y, z) + \sum_{j=1}^{6} {}^{A}\xi\Phi_j(x, y, z) \tag{3.7}$$

In order to resolve the eq. (3.7) we apply the below equations for every case in the wave.

Governing equation: $\nabla^2\phi = 0$ for $x,y,z \in R$ (3.8)

Free surface boundary condition: $-\omega^2\phi + g\frac{\partial\phi}{\partial z} = 0$ on $z = 0$ (3.9)

Bottom boundary condition: $\frac{\partial\phi}{\partial z} = 0$ on $z = -h$ (3.10)

Body boundary condition: $\frac{\partial\phi}{\partial n} = U_n$ on S (3.11)

The incident wave, radiation wave and diffraction wave can be obtained by Eq (3.12~3.14):

Incident wave: $\Phi_I(x, y, z) = -\frac{g}{\omega}\eta_0 e^{-ikx}e^{kz} = -\frac{g}{\omega}\eta_0 e^{-ik(x\cos\mu - y\sin\mu)}e^{kz}$ (3.12)

Radiation wave: $\Phi_R(x, y, z, t) = \sum_{j=1}^{6} {}^{A}\xi\Phi_j(x, y, z)e^{i\omega t}$ (3.13)

Diffraction wave: $\Phi_D(x, y, z, t) = \Phi_D(x, y, z)e^{i\omega t}$ (3.14)

The equation (3.15~3.17) show the general of forces and moment acting in vessels:

Force: $F = \iint_s Pn\, dS$ (3.15)

Moment : $M = \iint_S P\,(r \times n)\, dS$ (3.16)

$$F_j = \iint_S P n_j dS \quad j = 1, ...6 \tag{3.17}$$

In the first case, from the equation (3.7) we look for the forces of Radiation waves:

$$\Phi_R = (x, y, z, t) = \Phi_R(x, y, z)e^{i\omega t} = \sum_{j=1}^{6} \overset{A}{\xi}_j \Phi_j(x, y, z) \tag{3.18}$$

$$P_R = -\rho \frac{\partial \Phi_R}{\partial t} = -\rho i\omega \sum_{j=1}^{6} \overset{A}{\xi}_j \Phi_j(x, y, z)e^{i\omega t}$$

$$F_R = \iint_S P_R n \, dS$$

$$F_{R,k} = \sum_{j=1}^{6} \overset{A}{\xi}_j F_{jk} e^{i\omega t}$$

$$F_{jk} = -\rho \iint_S \Phi_j \frac{\partial \Phi_k}{\partial n} dS = \omega^2 A_{jk} - i\omega B_{jk}$$

The force of the Froude-Krylov (F_{FK}) and Diffraction force (F_D). Incident and Diffraction wave velocity potential:

$$F_{FK} + F_D = \iint_S (P_{FK} + P_D) n \, dS \tag{3.19}$$

$$F_{FK,k} + F_{D,k} = -\rho \iint_S (\Phi_I + \Phi_D) i\omega e^{i\omega t} n_k \, dS \tag{3.20}$$

The RAOs (Response Amplitude Operator) can be obtained Eq. (3.21):

$$M\ddot{X} = F_{Gravity} + F_{Static} + F_{F.K} + F_D + F_R \tag{3.21}$$

$$(M + A)\ddot{X} + B\dot{X} + CX = F_{exciting}$$

$$X^A = \eta_0 f^A \left[-\omega^2 (M + A) + iwB + C\right]^{-1} \tag{3.22}$$

with:

$$X = X^A e^{i\omega t} \tag{3.23}$$

$$\dot{X} = i\omega X^A e^{i\omega t}$$

$$\ddot{X} = -\omega^2 X^A e^{i\omega t}$$

$$F_{exciting} = \eta_0 f^A e^{i\omega t}$$

where, the variable are defined as follows:

η_0 : wave amplitude; f^A : wave exciting force Amplitude

3.3. Simulation condition

Numerical simulation have been carried out for KVLCC2. The principal particulars of KVLCC2 are listed in Table. 3.1. In this study, simulation are conducted to investigate the effect of regular wave on RAO motion of KVLCC2 in various wave directions. The wave condition for this simulation is listed in Table. 3.2. The simulation is performed for full scale ship of KVLCC2 and downloaded on the SIMMAN 2020. The loading conditions of design are listed in Table. 3.3.

Table 3.1 Principal particulars of KVLCC2

Item	Unit	full scale
Length between perpendiculars	m	320.0
Maximum beam of water line	m	58.0
Draft	m	20.8
k_{xx} $(0.4B)$	m	23.2
k_{yy} $(0.25L)$	m	80
k_{yy} $(0.25L)$	m	80

Table 3.2 Wave conditions

Speed of vessel [knots]	Wave direction [deg.]	Wave frequencies [rad/s]
0	0, 30, 60, 90, 120, 150, 180	0.4-2.5

Table 3.3 Loading conditions

Item	Unit	full scale
Longitudinal Center of Gravity from A.P	m	171.1
Vertical Center of Gravity from B.L (Base line)	m	18.6

3.4. Setup for numerical simulation

Computation of ship's motion of KVLCC2 are accomplished by performing frequency domain analysis in ANSYS AQWA (3D Panel method). ANSYS AQWA provides a tool set for investigating the effect of environmental loads on marine structures. The processing of solving the problem of ship motion in AQWA will be following the steps such as: Step 1, import IGS file downloaded from the SIMMAN website, define the water line, make each structure into a single part. Step 2, we carried out generate meshing. Step 3, Pre-processing: analysis setting, choose wave direction, wave frequencies, and ship's forward speed. Step 4, Solver. Step 5, Post-processing: export the result. Fig. 3.3~3.4 show the geometry and setup of the KVLCC2. In step 2, the quality of the discrete hull surface by constant panels will affect the accuracy of hydrodynamic properties of analyzing structures. For each individual panel must satisfy with the requirement in this program. Fig. 3.5 show the generated mesh of the KVLCC2 in AQWA of the KVLCC2 ship, the direction of wave and export the results. The mesh is automatically generated and its density based on maximum element size parameter.

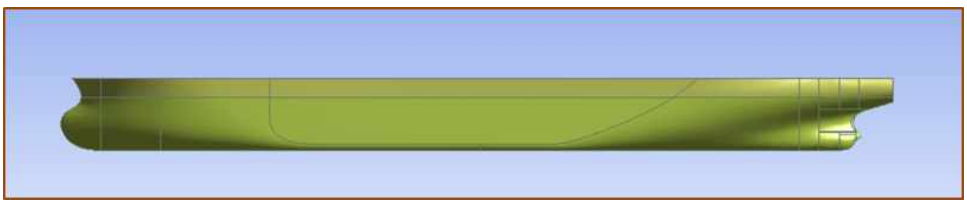

Fig. 3.3 Geometry of the KVLCC2

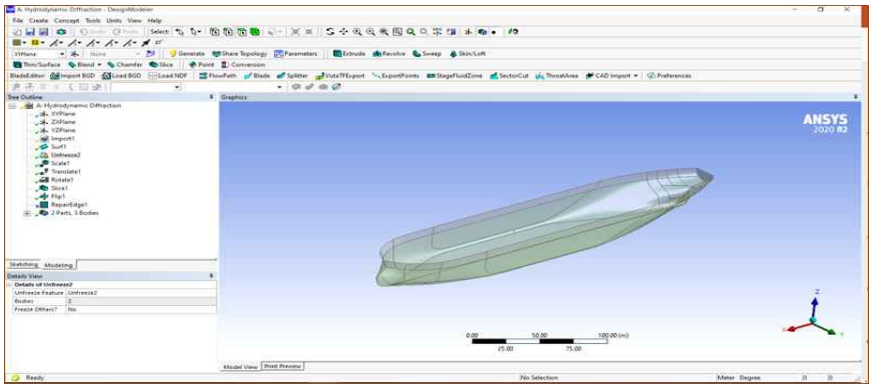

Fig. 3.4 Setup the full scale

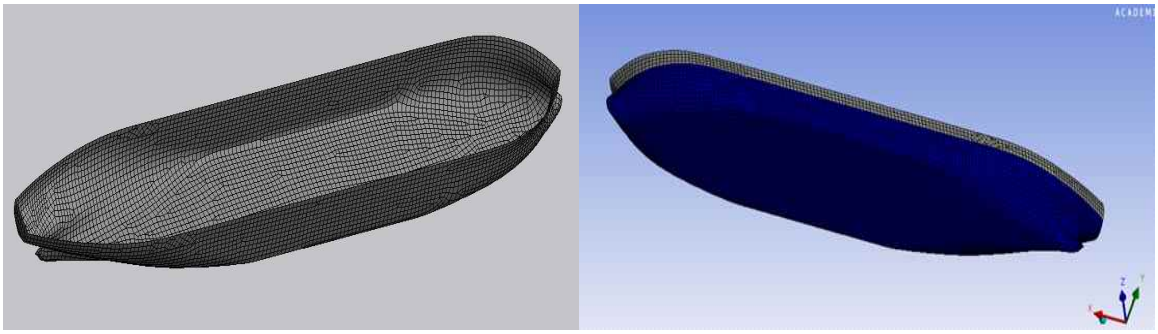

Fig. 3.5 Mesh generation of the model ship

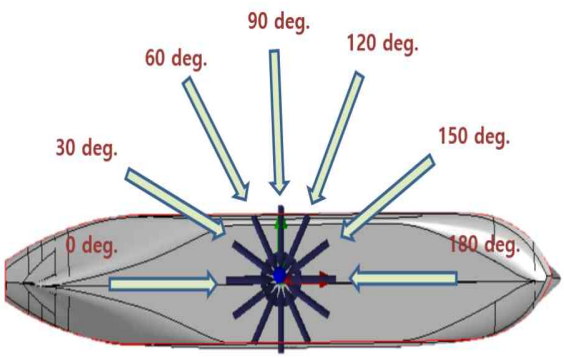

Fig. 3.6 Wave direction

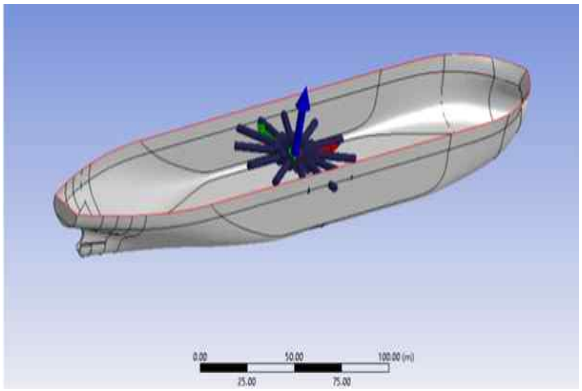

Fig. 3.7 Wave structure

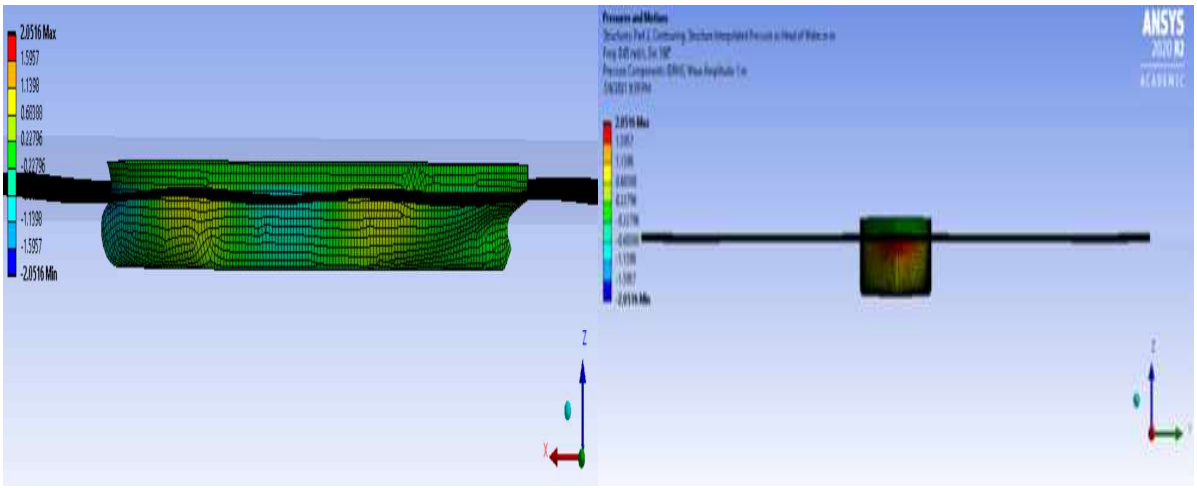

Fig. 3.8 Running and export

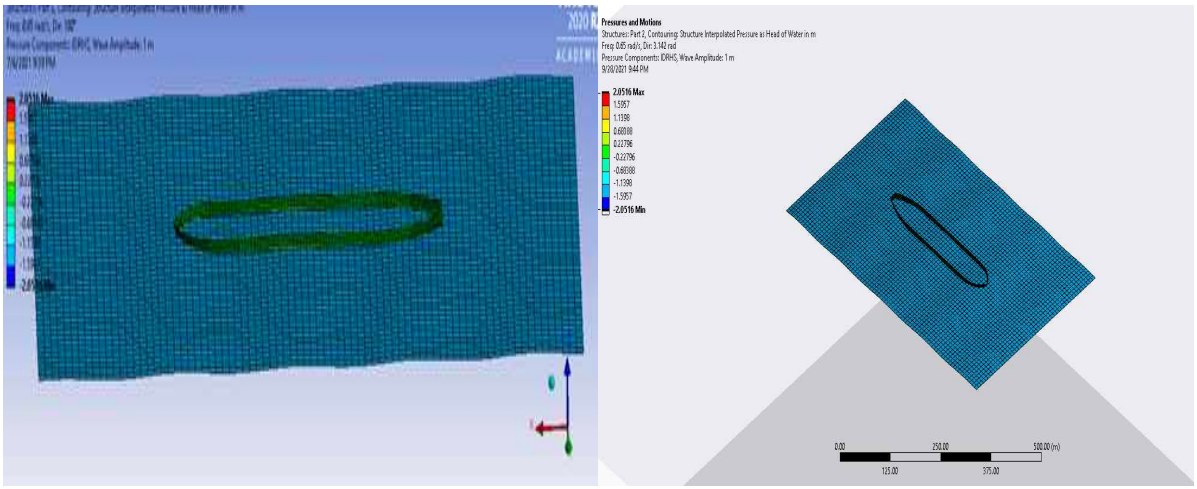

Fig. 3.9 Running and export result of the KVLCC2

3.5. Results and compare of simulation

3.5.1. Wave drift force

The wave drift force acting on an advancing KVLCC2 was evaluated by numerical method and experimental result. In this case, the wave drift force of the KVLCC2 was also used to measure zero forward speed. The 1/223 scale model and indirect method using tensiometers were used. Through this study, the data of the wave drift force acting on KVLCC2 were validated and the computation capability of the potential-based numerical method was systematically analyzed. Fig 3.10 shows wave drift force and moment depending on incident wave direction with respect to wavelength and different wave directions. It can be seen that the overall tendencies were very similar between the present results and another paper. The respective normalized coefficients of the steady drift forces and moment are defined as follows:

$$c_x = \frac{-F_x}{\rho g A^2 (B^2/L)},\ c_y = \frac{-F_y}{\rho g A^2 (B^2/L)},\ c_N = \frac{-M_z}{\rho g A^2 B^2} \tag{3.24}$$

where, L is ship length between perpendiculars, B is ship breadth at the water line.

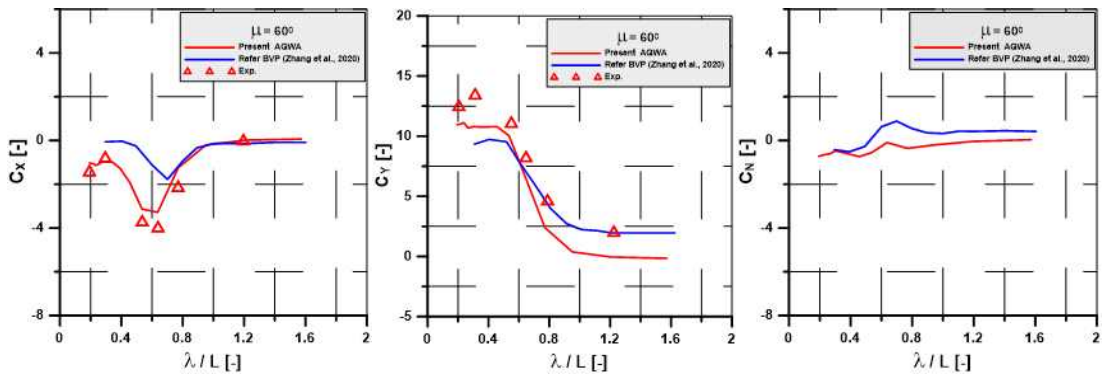

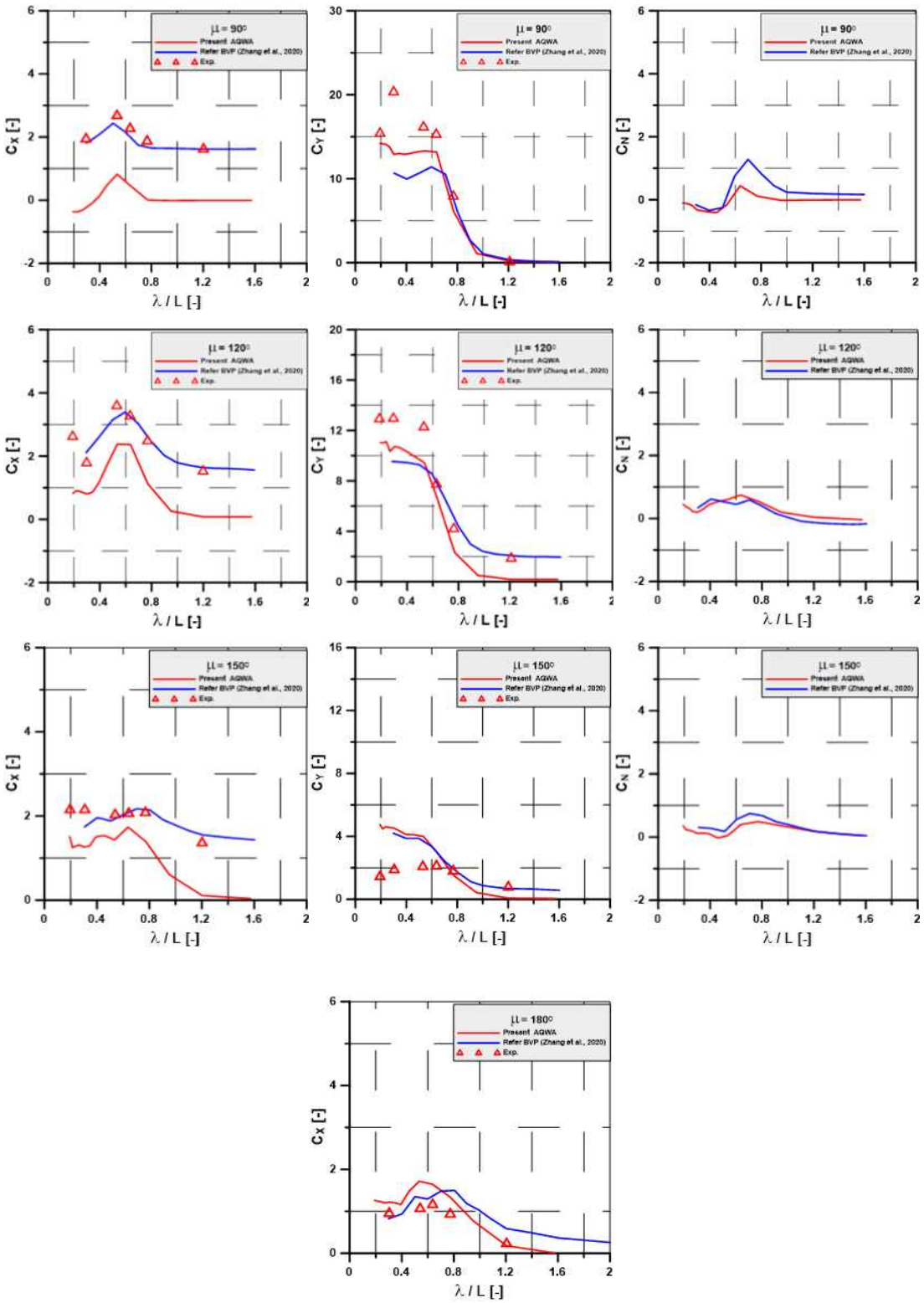

Fig. 3.10 Steady longitudinal force, steady transverse force, and steady yaw moment

3.5.2. Response Amplitude Operator (RAOs)

The motion of ships in the steadily translating $O(x,y,z)$ system are defined by translation motions and rotation motions. Three translations of the ship in the center of gravity in three direction of x, y and z axes. Three rotations of the ship about three directions of x, y and z axes. Three translations and three rotations are defined by Eqs. (3.24~29):

$$\text{Surge: } x = x_a \cos(\omega_e t + \varepsilon_x \zeta) \tag{3.24}$$

$$\text{Sway: } y = y_a \cos(\omega_e t + \varepsilon_y \zeta) \tag{3.25}$$

$$\text{Heave: } z = z_a \cos(\omega_e t + \varepsilon_z \zeta) \tag{3.26}$$

$$\text{Roll: } \phi = \phi_a \cos(\omega_e t + \varepsilon_\phi \zeta) \tag{3.27}$$

$$\text{Pitch: } \theta = \theta_a \cos(\omega_e t + \varepsilon_\theta \zeta) \tag{3.28}$$

$$\text{Yaw: } \psi = \psi_a \cos(\omega_e t + \varepsilon_\psi \zeta) \tag{3.29}$$

where, ε is the different phase between motion and incident wave. The respective normalized coefficients of translations and rotations are defined as follows:

$$\text{For translations: } RAO = \frac{x,y,z}{\zeta_A} \tag{3.30}$$

$$\text{For rotations: } RAO = \frac{\phi,\theta,\psi}{k\zeta_A} \tag{3.31}$$

where, the variable are defined as follows:

ζ_A: wave amplitude

k: wave number

Table 3.4 Natural frequency

Item	Unit	KVLCC2
Heave natural frequency	rad/s	0.506
Roll natural frequency	rad/s	0.293
Pitch natural frequency	rad/s	0.527

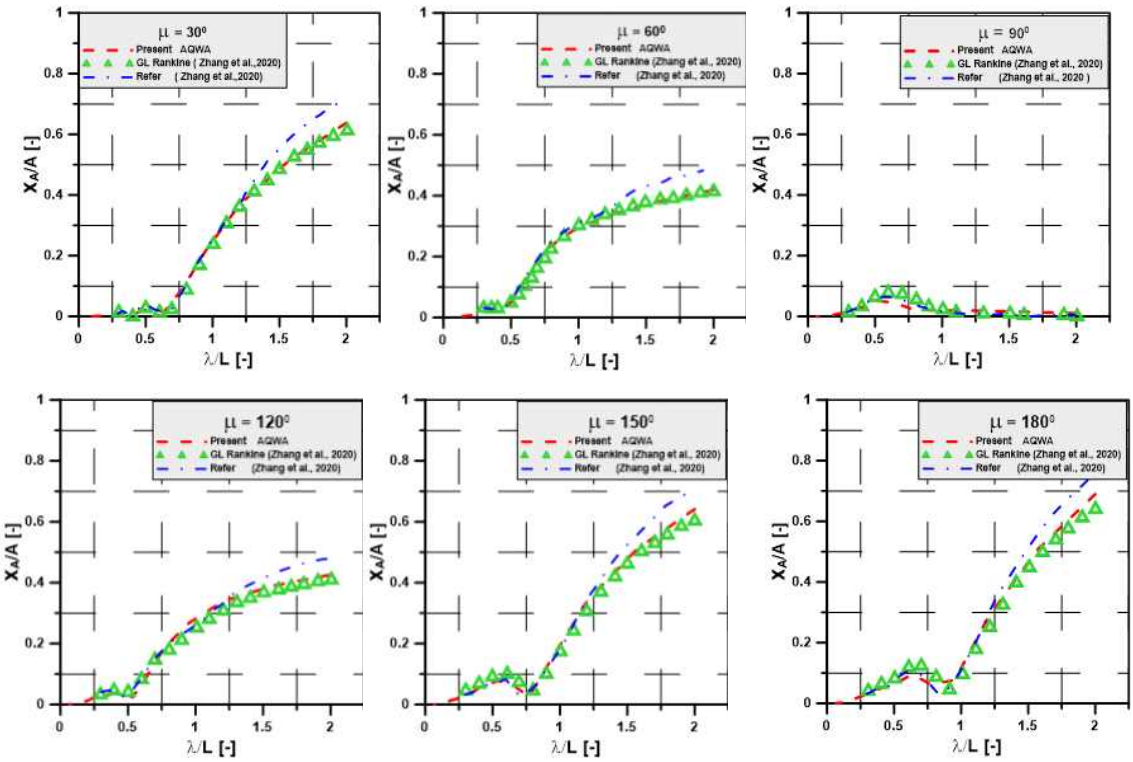

Fig. 3.11 Surge motion RAOs of KVLCC2

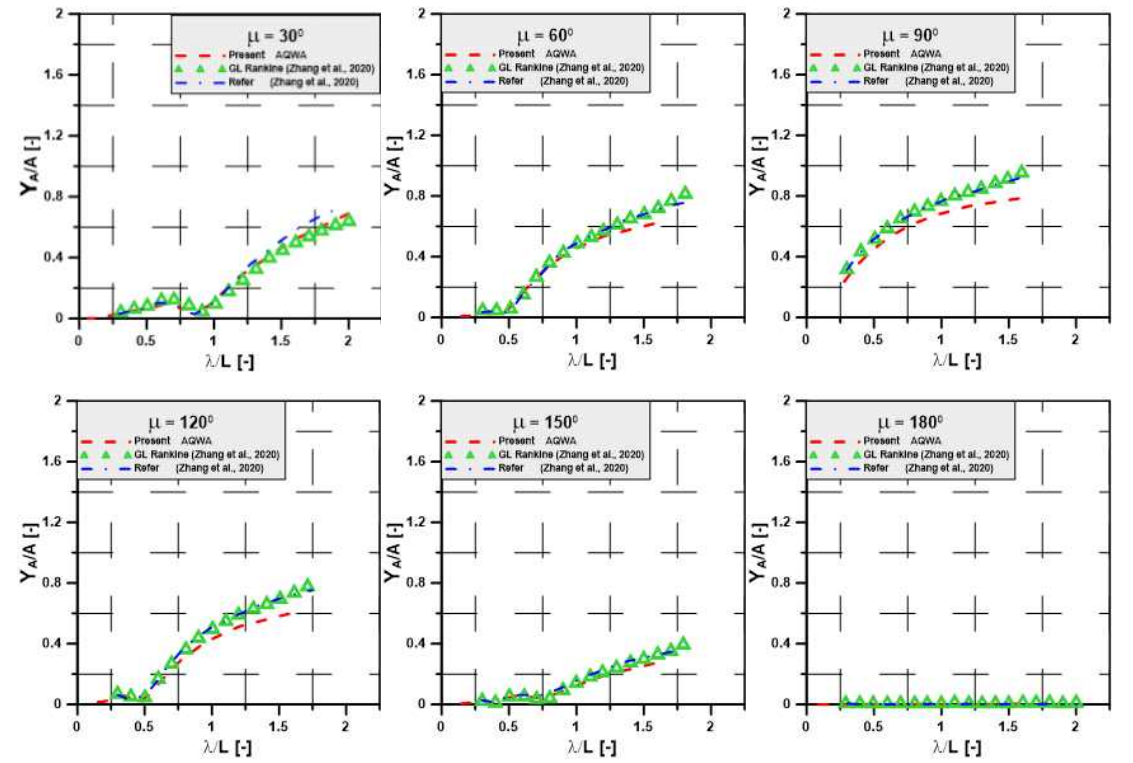

Fig. 3.12 Sway motion RAOs

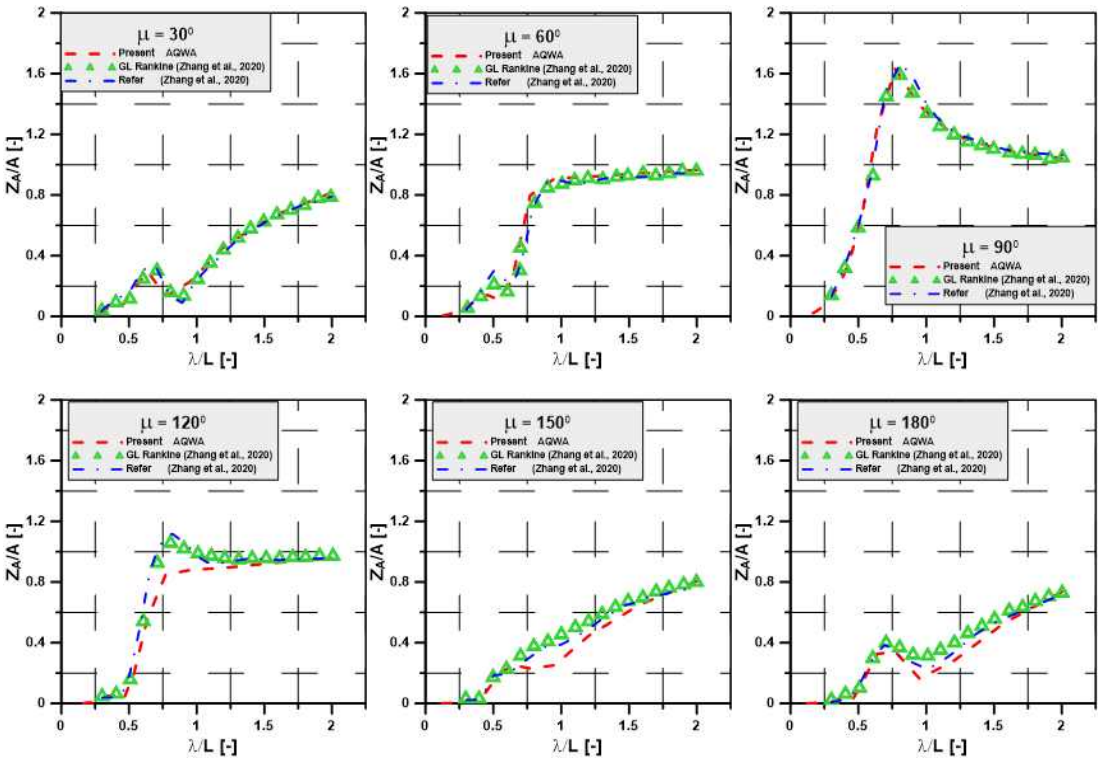

Fig. 3.13 Heave motion RAOs

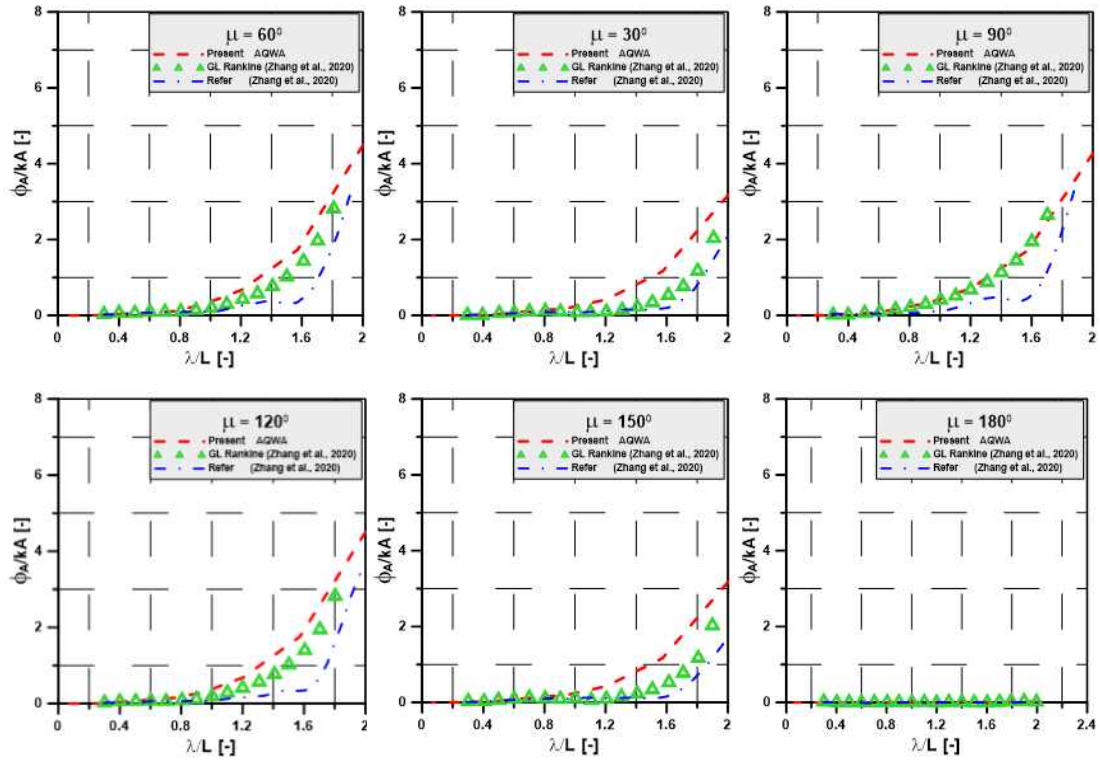

Fig. 3.14 Roll motion RAOs

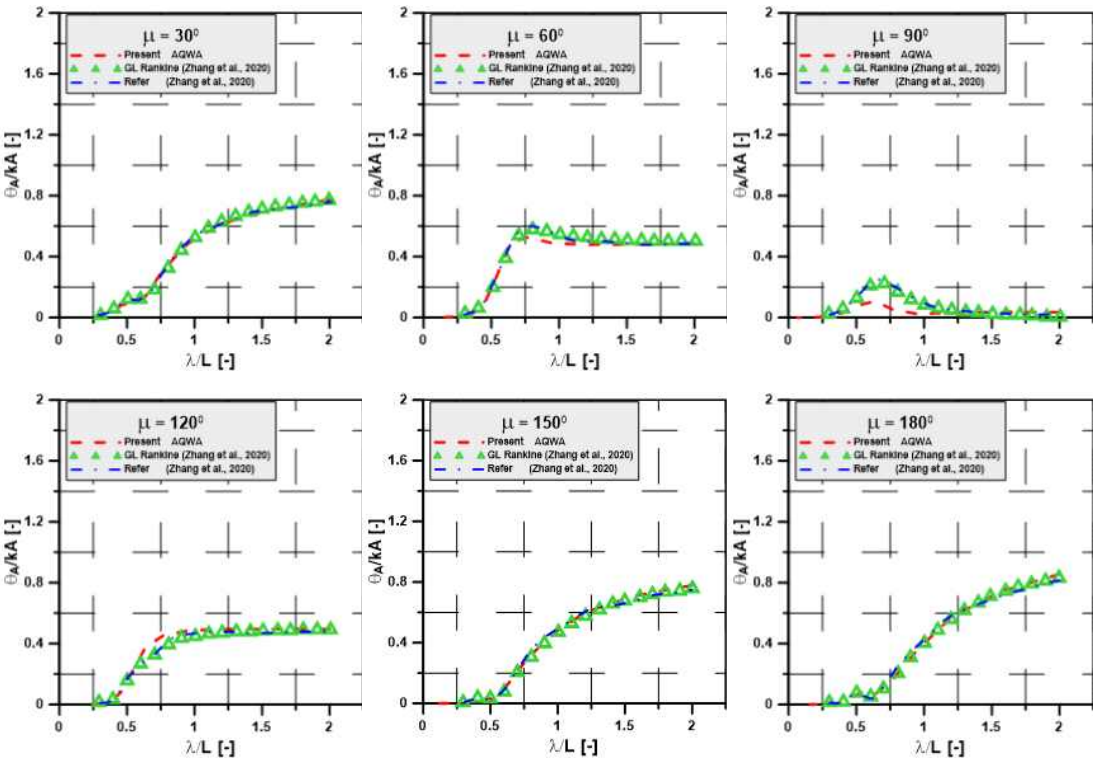

Fig. 3.15 Pitch motion RAOs

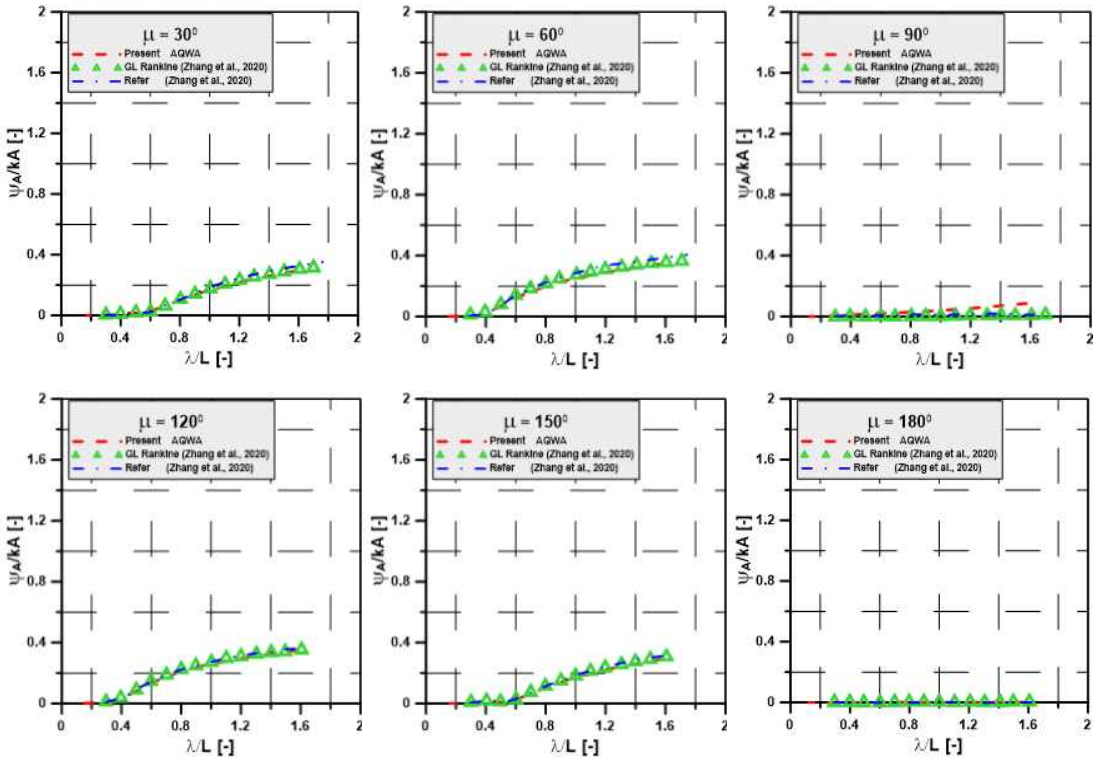

Fig. 3.16 Yaw motion RAOs

The model test was conducted on regular wave to evaluate the motion of the KVLCC2. The motion responses of KVLCC2 in regular waves are investigated in various wave directions with the range of λ/L from 0.5 to 2.0. The largest surge RAO of KVLCC2 occurs when the wave direction approaches to 0 degrees and 180 degrees. Surge RAO decreases as the wave direction approaches to 90 degrees as shown in fig. 3.11. In contrast to surge RAO, the sway RAO is greatest when the wave direction reaches to 90 degrees and it is the smallest in the case of following sea and head sea as shown in Fig. 3.13. shows the heave RAOs of KVLCC2. Heave RAO increases when the wavelength increases. In addition, when the wave direction changes, the heave RAO changes slightly. The largest roll RAO of KVLCC2 occurs when the wave direction approaches to 90 degrees. Roll RAO decreases as the wave direction approaches to 0 degrees and 180 degrees as shown in fig. 3.15. In contrast to surge RAO, the pitch RAO is the smallest in case of beam sea and it is the greatest when the wave direction reaches to 0 degrees and 180 degrees. The heave RAO, pitch RAO and roll RAO increase when the wavelength increases. Fig. 3.16. shows the yaw RAO of KVLCC2 and yaw RAO is dominant in oblique wave and is the smallest in beam sea and following.

4. Experimental method

4.1. Test facilities and test conditions

4.1.1. Test facilities

The experiment of KVLCC2 was carried out in the square wave tank in Changwon National University. As shown in Figure 4.1. The length and width of the towing tank were 20m and 16m, respectively, and the depth was 1.8m. In this experiment, the water depth was set 1.5m. Piston type wave makers were installed along the short sides and wave absorption beaches were located on the opposite sides. The absorption is used to absorb waves generated by wave makers and eliminate reflected waves. The wave maker could made waves with the height up to 20cm, and a wavelength to 3m. The towing carriage fixed in the center of the tank as well as the model ship will be fixed in the carriage and changed the direction of the model ship. The maximum carriage speed is 1.0 m/s. Fig. 4.2 shown the wave maker and observer of tank.

Fig. 4.1. Wave tank in CWNU

Fig. 4.2. Wave markers and absorptions

Table 4.1 Device used in this experiment

Items	Measurement
OptiTrack	Surge, sway, heave, roll, pitch, yaw
Tension gauge	Tension
IMU	Roll, pitch, yaw

In this experiment, the optical-based system OptiTrack V120:TRIO which were made by NaturalPoint company, were used to measure the six degree of freedom of the KVLCC2 ship. The tension gauge were used to measured and connected of spring. In addition, an inertial measurement unit (IMU) was used to measure attitude of the KVLCC2 ship. The device used in the present experiment are listed in Table 4.1.

Fig. 4.3. OptiTrack device

Fig. 4.4 Inertial measurement unit (IMU) device

Fig. 4.5 Tension gauge device

Fig. 4.6 A/D converter

Fig. 4.6 shows A/D converter NI USB-6212 which used in this experiment was made by National Instruments Corporation. It will convert the electrical signal of the output of tension gauge and wave probe into digital signals.

4.1.2. Model test

The KVLCC2 model test was selected to conducted to evaluate the wave drift force acting on a KVLCC2 model in the towing tank of Changwon National University. The second purpose of the model test was to calculate and investigate the RAO (Response Amplitude

Operator) under various wave directions of KVLCC2 model. The 1/223 scaled model of KVLCC2, as shown in Fig. 4.7. Figure 4.8 the wood plane attached in stern and bow of KVLCC2 ship, It's used to connect the springs and tension gauge. Additionally, Only the bare hull was considered without the propeller and rudder system. The principal particular of the full model and scale model of the KVLCC2 model are summarized in table 4.2.

Table 4.2 Principal particular of KVLCC2.

	Symbol	Unit	Full model	Scale model
Scale ratio			1	223
Length between perpendiculars	Lpp	m	320	1.435
Beam overall	Bwl	m	58	0.260
Depth	D	m	30	0.135
Draft	T	m	21	0.093
Displacement volume	∇	km^3	312622	1401.9
Weight displacement	W	kgf	320678340	28.917
Block Coefficient	C_B	m	1	0.810
Longitudinal Center of Gravity from A.P	LCG	m	171	0.767
Vertical Center of Gravity from B.L	VCG	m	2	0.008
Metacentric height transverse	GMt	m	6	0.026
Metacentric height longitudinal	GMl	m	38	0.170
Water density	ρ	kg/m^3	998	998.2
Gravity	g	m/s^2	10	9.810
Water plane area	Aw	m^2	27711	0.557

Fig. 4.7 Experimental model of KVLCC2

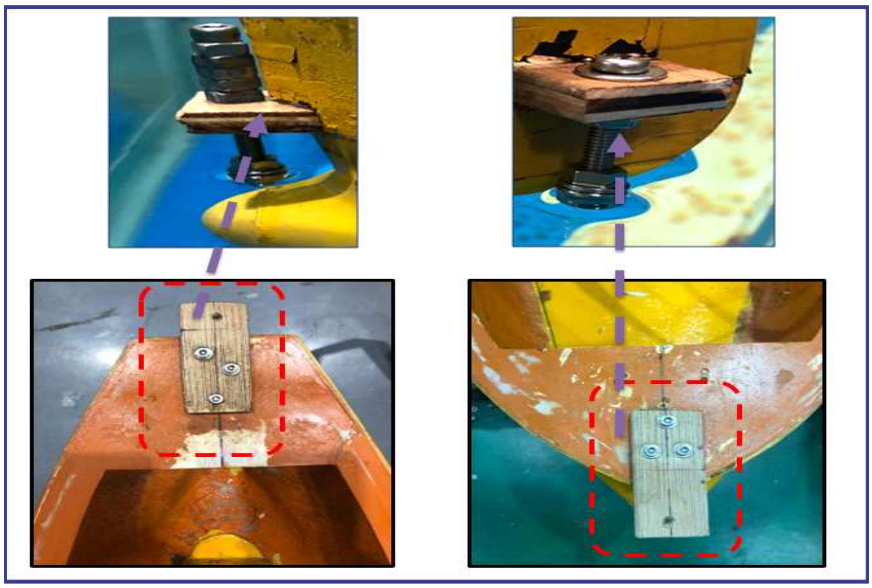

Fig. 4.8 Configuration of model test.

4.2. Test conditions

In this study, the model test was performed in the various wave directions with the ship speed set at zero. The wave direction was selected in 45^0 intervals from the head sea condition 180^0 to the following sea condition 0^0. In the Changwon National University tank the wave maker was installed at the end of the towing tank and the wave

directions changed by carriage. Fig. 4.9 shows setup for test. Experiment was conducted to investigate the effect of the wave drift force and wave on the motion response in various wave directions at zero speed. Thus, in case of the regular wave, refer from the ITTC-Recommended procedures and guidelines 'Seakeeping experiments' the ratio of the range of wave length to the ship length λ/L is carried 0.5 L_{PP} to 2.0 L_{PP}. The regular wave conditions of the full model and scale model for this experiment are listed in tables 4.3. In addition, the wave heights at the prow and aft parts of the ship were measured to review the incident wave are presented in table 4.4 The natural frequency of heave, roll and pitch listed in Table 4.5.

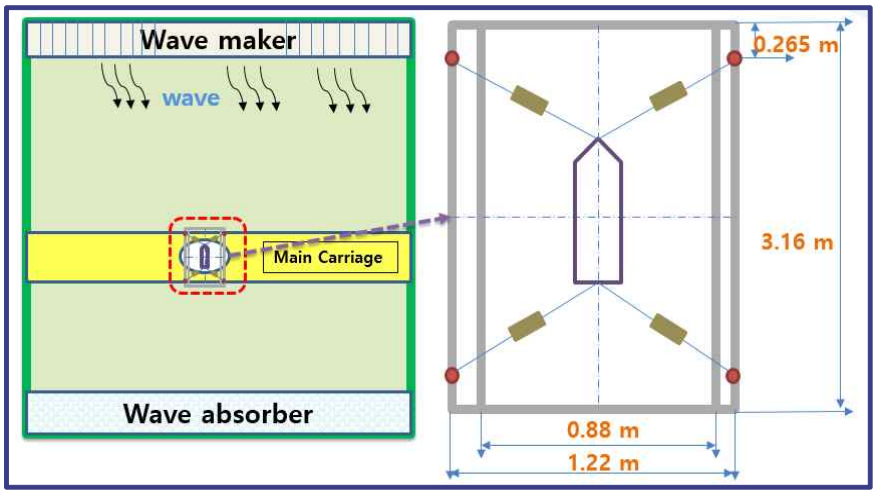

Fig. 4.9 wave calibration setup

Table 4.3 Regular wave conditions of the full model and scale model.

Full scale					Model scale				
Lambda/ L	Lambda	Period	Freq. (Hz)	Freq. (rad/s)	Lambda/ L	Lambda	Period	Freq. (Hz)	Freq. (rad/s)
0.50	160	10.123	0.099	0.621	0.50	0.717	0.678	1.4752	9.2687
0.75	240	12.398	0.081	0.507	0.75	1.076	0.830	1.2045	7.5678
1.00	320	14.316	0.070	0.439	1.00	1.435	0.959	1.0431	6.5539
1.25	400	16.006	0.062	0.393	1.25	1.794	1.072	0.9330	5.8620
1.50	480	17.534	0.057	0.358	1.50	2.152	1.174	0.8517	5.3513
1.75	560	18.939	0.053	0.332	1.75	2.511	1.268	0.7885	4.9543
2.00	640	20.246	0.049	0.310	2.00	2.870	1.356	0.7376	4.6343

Table 4.4 Wave height

Full model (m)	Scale model (m)	Scale model (cm)
3.2	0.0143	1.435
4.8	0.0215	2.152
6.4	0.0287	2.870
8.0	0.0359	3.587
9.6	0.0430	4.305
11.2	0.0502	5.022
12.8	0.0574	5.740

Table 4.5 Nature frequency

Motion	Full scale (rad/s)	Model scale (rad/s)	Period
Heave natural frequency	0.6505	9.7134	0.6469
Roll natural frequency	0.2892	4.3183	1.4550
Pitch natural frequency	0.1706	2.5481	2.4658

The nature frequency of heave, roll and pitch:

$$\omega_z = \sqrt{\frac{\rho g A_w}{2m}} \qquad \omega_\Phi = \sqrt{\frac{mgGM_T}{1.25 I_{xx}}} \qquad \omega_\theta = \sqrt{\frac{mgGM_L}{2I_{yy}}} \tag{4.1}$$

ω_z, ω_Φ, ω_θ: Nature frequency of heave, roll, pitch, respectively

I_{xx}, I_{yy} : Moment of inertia longitudinal, transverse

A_w : Water plane area

4.3. Experimental method

In this experiment, before proceeding with setup and performing the experiment, the KVLCC2 model will be conducted for some test as ballasting test, inertia test, inclining test and swing test to get the inertial values. The tension gauge and wave probe device was calibrated in order to convert the initial results. It was used to connect with the data after measured to analysis data.

4.4. Pre-test

4.4.1. Ballasting and inertia test

The mass dispensation of the KVLCC2 was checked to an exact match with the real model scale. Fig. 4.10 shows the ballasting of the model KVLCC2 ship. Besides, the inertia table and inertia swing was used to estimated the mass moment of inertia.

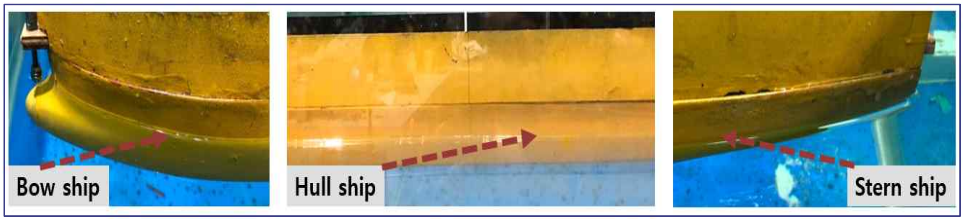

Fig. 4.10. Ballasting of model KVLCC2 ship.

Table 4.6 Inertia table test result of KVLCC2

Weight 1 [kg]	Weight 2 [kg]	X [m]	T [sec.]	Inertia of moment [kgm^2]
4	4	0.05	1.08	0.02
4	4	0.1	1.41	0.08
4	4	0.15	1.88	0.18
4	4	0.2	2.36	0.32

Table 4.7 Inertia table test result of KVLCC2

Item	1st
Coef._a	0.10
Coef._b	-0.12
Coef._c	0.03
J_measured	3.76
T	6.71

Item	Unit	Value
Lpp	m	1.43
kzz	m	0.36
m	kg	28.15
J_target	kgm^2	3.62
J_measured		3.76
Difference	%	3.81

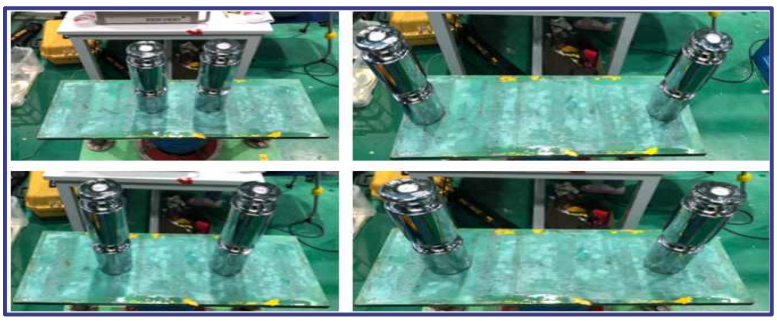

Fig. 4.12. Calibration inertia table test

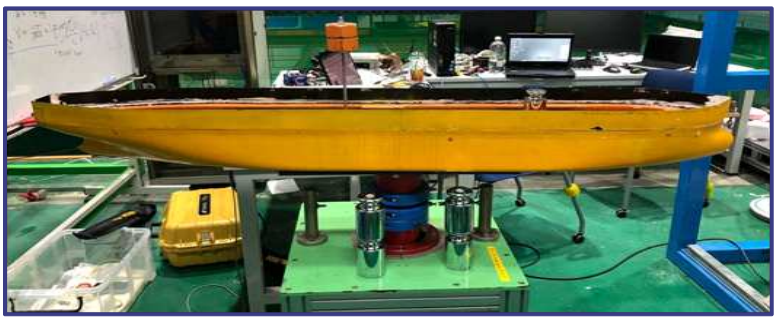

Fig. 4.11. Inertia table test

The estimation of the moment of mass inertia of the ship:

$$I_s = -m_s l_s^2 - B + \frac{T_s^2}{4\pi^2}(m_s l_s g - A) \tag{4.2}$$

A, B: Estimation coefficient of moment of mass inertia

m_s, l_s: Input value

T_s : Measurement value

Table 4.8 Inertia swing test result of KVLCC2

Item	Value
A	-131.22
B	13.28
Is [kgm^2]	3.73
Is_estimation [kgm^2]	3.62
Difference [%]	3.06

Input measurement	Weight 1	Weight 2	Ship
m[kg]	10	20	28.15
l[m]	0.93	0.93	0.895
T[s]	1.973	1.962	2.032
C	13.575	19.255	

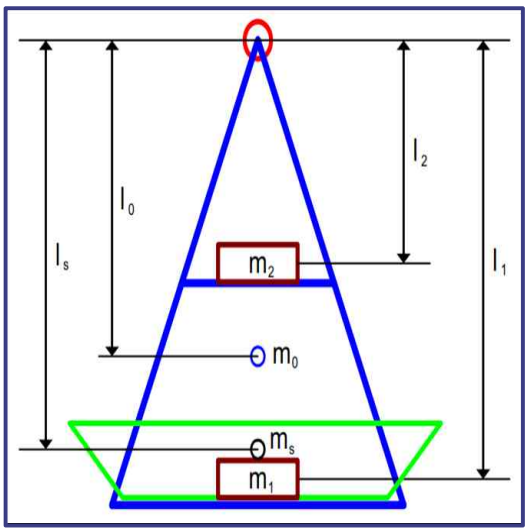

Fig. 4.13 Definition of a symbol

Fig. 4.14 Inertia swing test

4.4.2.Inclining test

After ballasting test was completed, an inclining test was carried out to check the transverse metacenter height (GM_T). The inclining test confirms the inclination angle when the mass in the model ship is moved in the horizontal direction and adjusts the height of the weight attached to the stern side of ship. During ballasting test of the model ship, it is convenient to attach the digital protractor(inclinometer sensor) to the model ship and perform ballasting together. GM_T is the distance from the ship's center of gravity (G) to the metacenter height (M) and the case where the M is above G is defined as a positive value. Fig. 3.18, the position of the GM_T is determined by the displaced hull shape of the hull, and buoyancy center (B) is determined by the displacement of the ship.

Table 4.9 Inclining test result of KVLCC2

Items	Model
Mass [kg]	28.15
GM [m]	0.03
Moved weight [kg]	2
Lever ly [m]	0.05
Heel angle (deg.)	7.90

Items	Measured value [deg.]	Heal angle [deg.]	Error [%]
Start point measured	0.06	-	-
Move weight to Port	7.81	7.75	1.87
Move weight to Starboard	7.76	7.7	2.50

$$GM_T = \frac{\omega l_y}{W \bullet \tan\Phi} \quad \Phi = \tan^{-1}\left(\frac{\omega l_y}{W \bullet GM_T}\right) \tag{4.3}$$

GM: Metacentric height (m)

ω: Moved weight (kg)

W: Mass of ship (kg)

Φ: Heel angle (deg.)

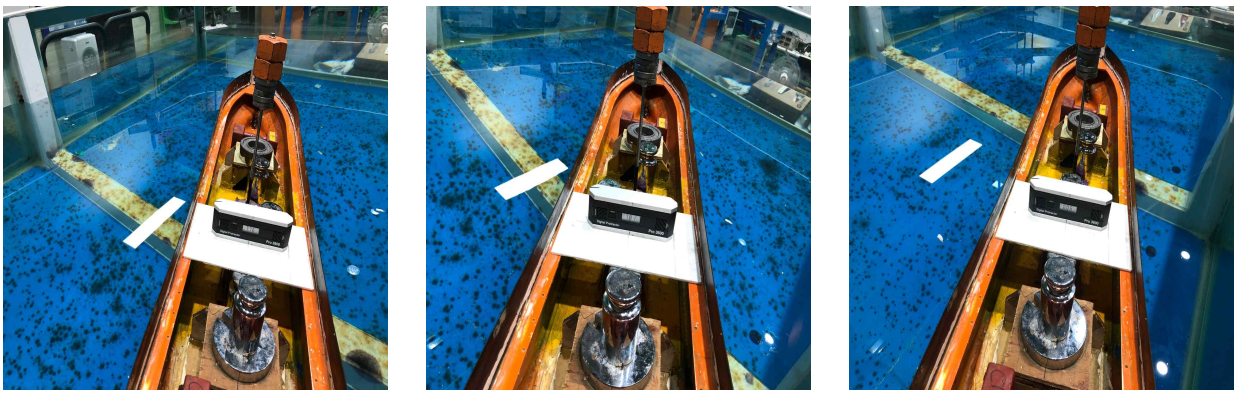

a, Move weight to STBD b, Initial state c, Move weight to Port

Fig. 3.15 Results of inclining test

4.4.3. Calibration of tension gauge

As such ballasting test, inclining test and inertia test. It is necessary in order to calibrate the sensors to measure physical quantities during the model test after distributing the mass of the model ship. The tension gauges were measured the wave force acting on the ship model of KVLCC2. It is connected to the ship at four angle positions by cable lines and springs. Two tension gauges were connected to the ship's bow, whereas the other two tension gauges were connected to the ship's stern. Fig. 4.16 shows the pictures of tension gauges calibration, the analog signal was measured by different weights and placed weights in the vertical direction. The ouput signal is amplified by an amplifier device, an analog signal is converted to a digital signal using A/D converter, and the digital signal resutls then displayed in computer. Fig. 4.17 shows the relationship between measuring tension and the output voltage of the amplifier. Eq. (4.4) expresses the calibration coefficient matrix for the tension gauges. Table 4.10 shows the measured results with different weights.

Fig. 4.16 Calibration of tension gauge

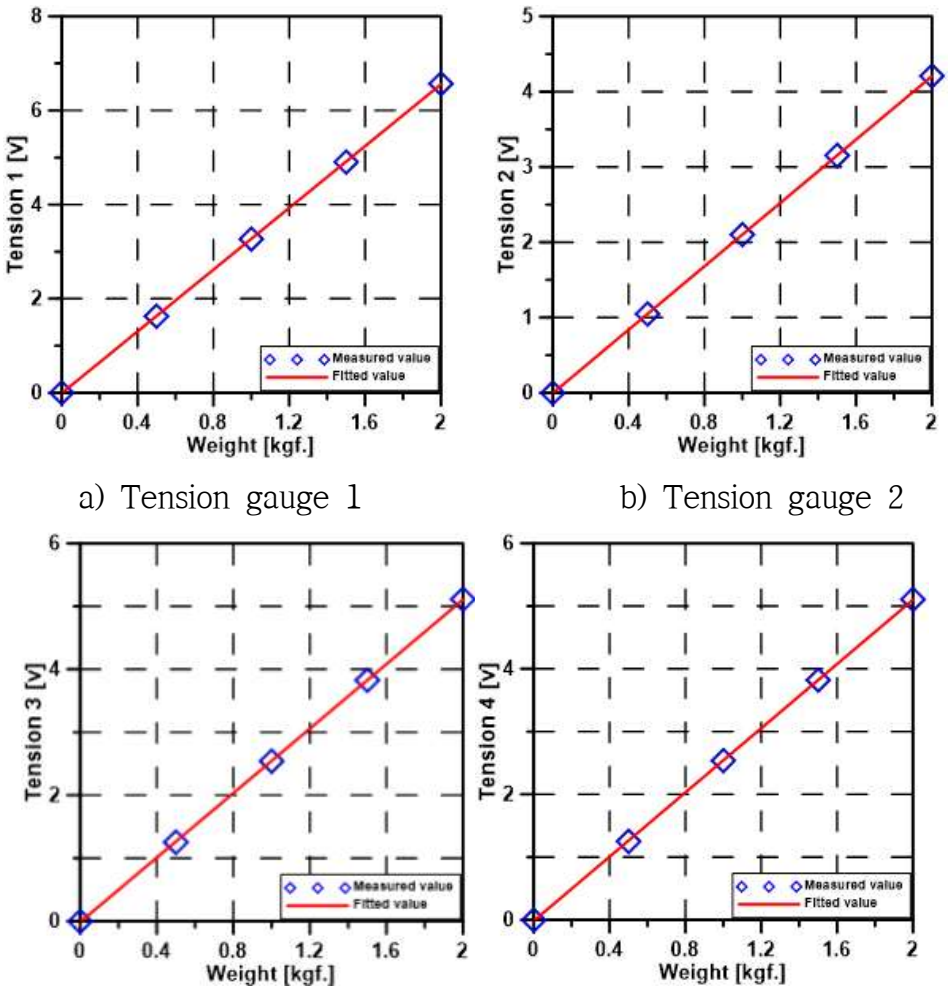

a) Tension gauge 1 b) Tension gauge 2

c) Tension gauge 3 d) Tension gauge 4

Fig. 4.17 Results calibration of tension gauges

Table 4.10 Results calibration of tension gauges

Tension Gauge	Weight [kgf.]	Measured TG01 [V]	Measured TG02 [V]	Measured TG03 [V]	Measured TG04 [V]
TG _0	0	0.0012343	-0.0023	-0.001937	-0.004847
TG _1	0.5	1.629691	1.047329	1.2550069	1.250964
TG _2	1	3.2679515	2.101134	2.5414832	2.537924
TG _3	1.5	4.9048869	3.153033	3.8265216	3.821721
TG _4	2	6.568608	4.208441	5.1130211	5.108052

$$\begin{bmatrix} T_1 \\ T_2 \\ T_3 \\ T_4 \end{bmatrix}(N) = \begin{bmatrix} 5.370 & 0 & 0 & 0 \\ 0 & 5.499 & 0 & 0 \\ 0 & 0 & 5.439 & 0 \\ 0 & 0 & 0 & 5.324 \end{bmatrix} \begin{bmatrix} T_1 \\ T_2 \\ T_3 \\ T_4 \end{bmatrix}(V) \tag{4.3}$$

4.4.4. Calibration of wave probe

Fig. 4.18 shows the wave probe calibration setup including a capacity type wave probe, amplifier that amplifies measured signal, A/D converter to convert analog signal to digital signal and DAQ (Data AcQuisition) computer. Fig. 4.19 shows the results of the wave probe calibration test was selected.

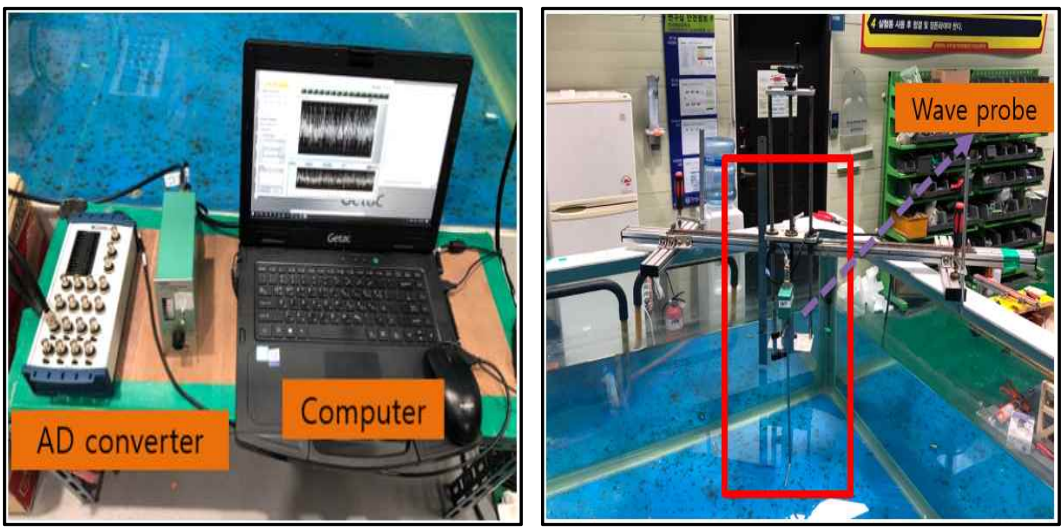

Fig. 4.18 Wave probe calibration

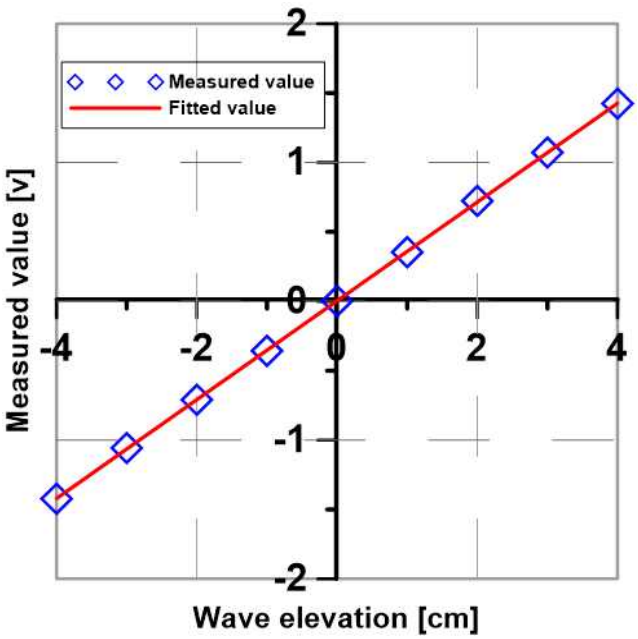

Fig. 4.19 Results of wave probe calibration

4.4.5. Wave maker calibration

Wave maker calibration is necessary in order to find the relationship between the wave height input in the wave generator program and the actual wave height to obtain the correction factor for the input wave height of the wave maker system for each wave frequency. It is necessary to evaluate the quality of the waves under various wave directions and wave frequencies (ITTC, 2017). The regular wave calibration was performed by inputting different wave heights for each frequency into wave generator program. In this experiment, the wave maker calibration test for 7 frequencies was carried out. Fig. 4.20~4.21 shows the real wave calibration setup and results of the relationship between input wave maker stroke and the measured wave height for RW01~RW07 of the regular wave described in table 4.11.

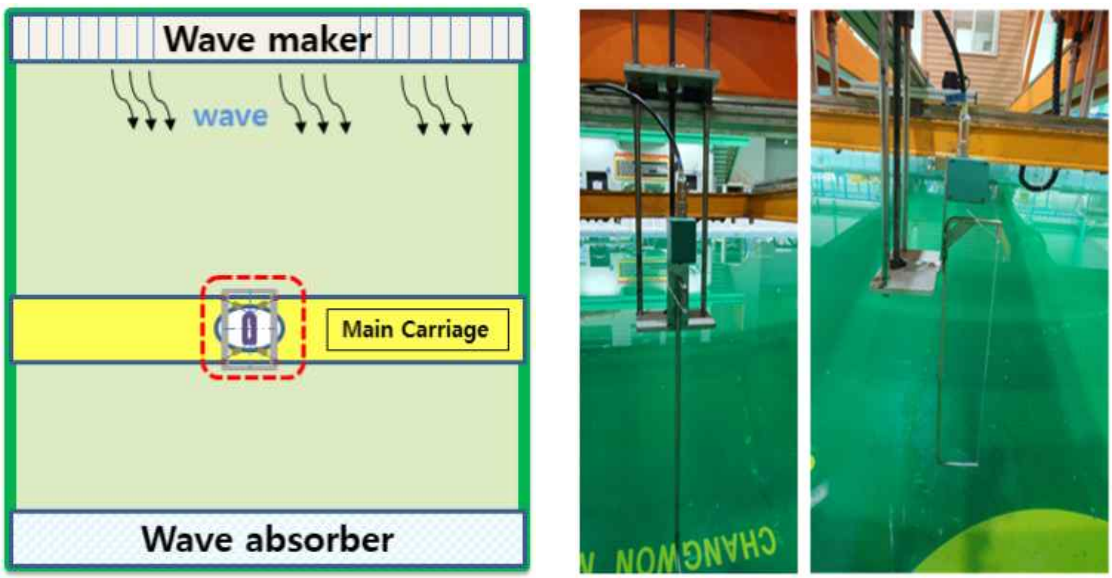

Fig. 4.20 Wave calibration setup in tank

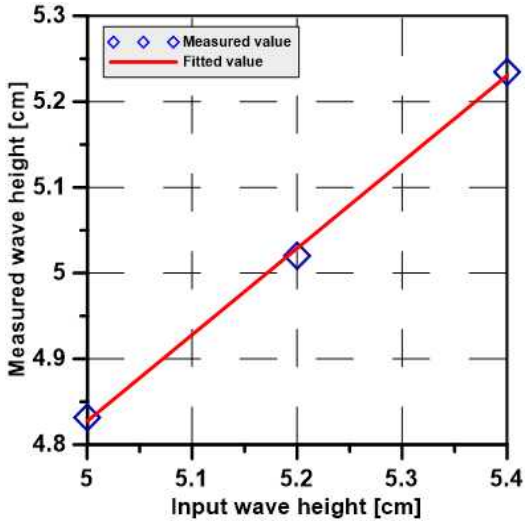

a) $\omega = 9.26$ rad/s

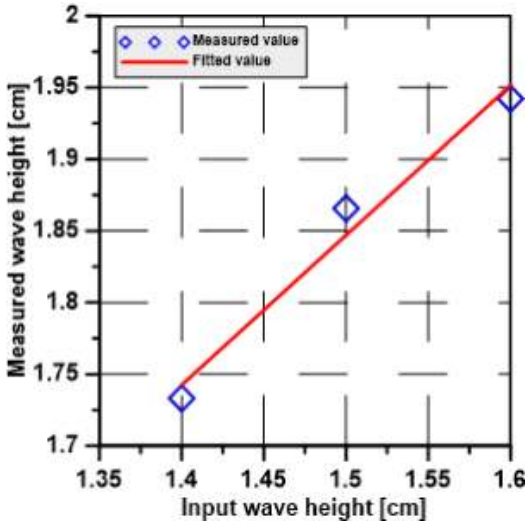

b) $\omega = 7.56$ rad/s

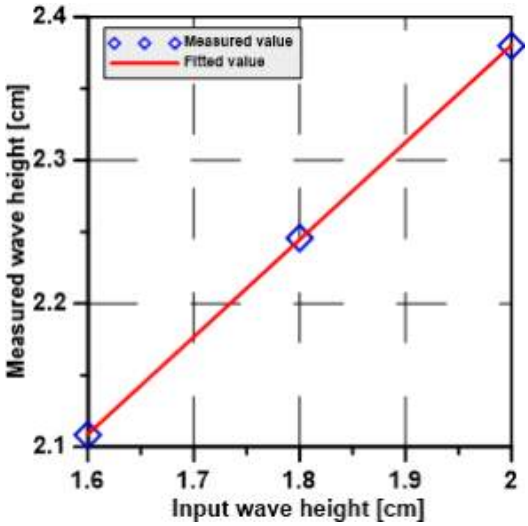

c) $\omega = 6.55$ rad/s

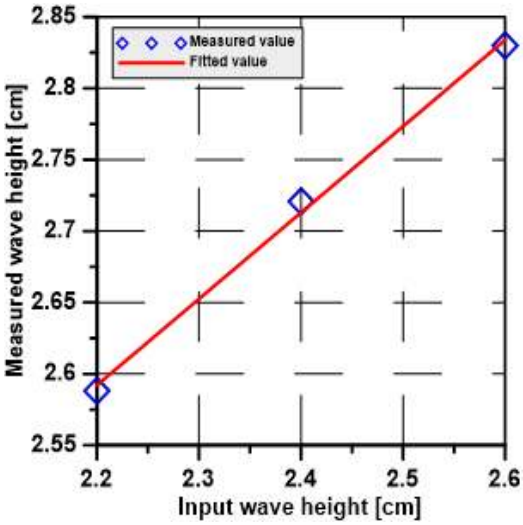

d) $\omega = 5.86$ rad/s

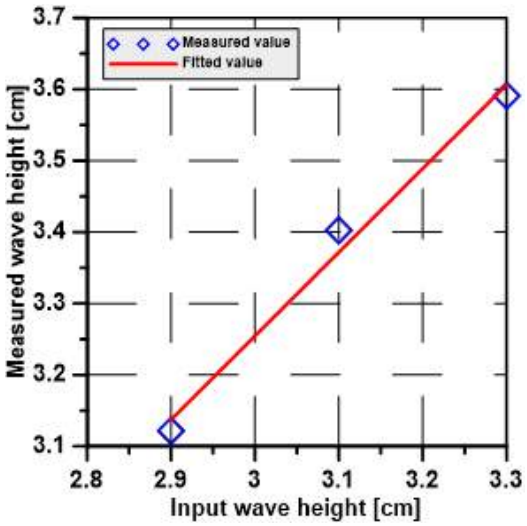

e) $\omega = 5.35$ rad/s

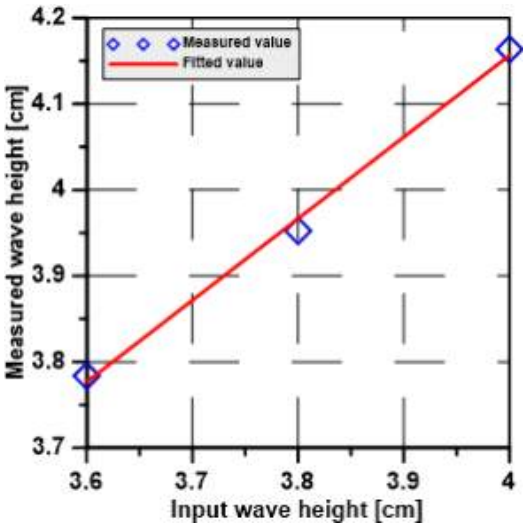

f) $\omega = 4.95$ rad/s

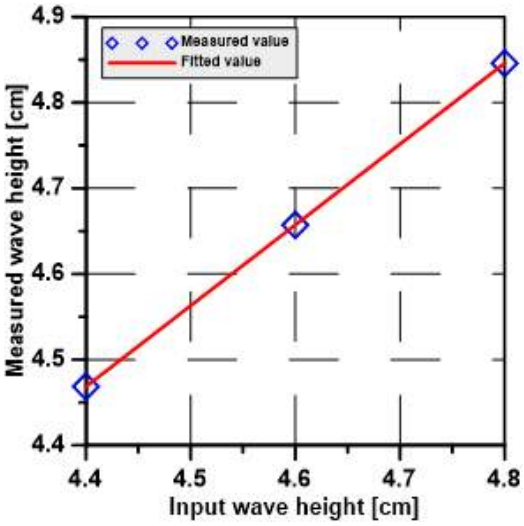

g) $\omega = 4.63$ rad/s

Fig. 4.21 Tension gauge calibration results

Table 4.11 Target wave height and input wave maker stroke

λ/L [-]	Wave Frequency (rad/s)	Target wave height (cm)	Input stroke (cm)	Measured wave height (cm)	Difference (%)
0.50	9.26	1.43	1.11	1.47	2.45
0.75	7.56	2.15	1.66	2.16	0.19
1.00	6.55	2.87	2.66	2.89	0.81
1.25	5.86	3.59	3.28	3.57	0.52
1.50	5.35	430	4.16	4.29	0.31
1.75	4.95	5.02	4.99	4.99	0.58
2.00	4.63	5.74	5.91	5.63	1.88

4.5. Experimental setup

4.5.1. Setup for model ship

Before installing model, on the carriage pre-installed the aluminium frame with the length and width of the frame were 2.64m and 1.08m, respectively. In addition, the model was connected with the mooring lines, springs and tension gauges after measurement sensor were completed. As shows in fig. 4.22, the model ship was installed in a state where 6-DOF motion is free by applying the soft mooring spring. After install models was finished, the tension gauges at four angle points should be connected with mooring lines and springs to the model KVLCC2 ship. At this time, it is necessary to check the pretension to the tension gauge and measure the force when the model ship shakes by giving a force to the tension gauge. Fig. 4.23 describes the model ship installation schematic of the model in tank.

Fig. 4.22 installation of model ship

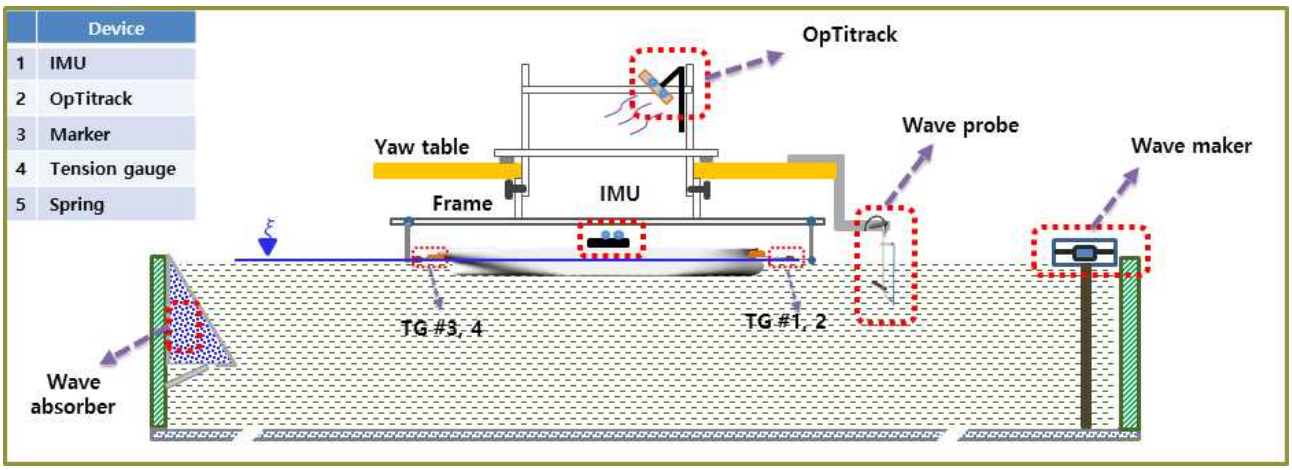

Fig. 4.23 Diagram of experiment setup

4.5.2. Setup of measurement device

Fig. 4.24 shows the OptiTrack were installed on top the frame and look down with the camera unit and makers in the model ship. The camera unit was installed with the distance so that it can catch the makers well. Besides, the black tape covers the model and frame in order to remove the unwanted optical noise because the camera unit would identify any white color as a maker. On the other hand, the wave probe was installed in front of the model ship in 3D wave tank. Fig. 4.25 describe data acquisition configuration of the measurement sensors was installed on the carriage.

Fig. 4.24 OptiTrack installation

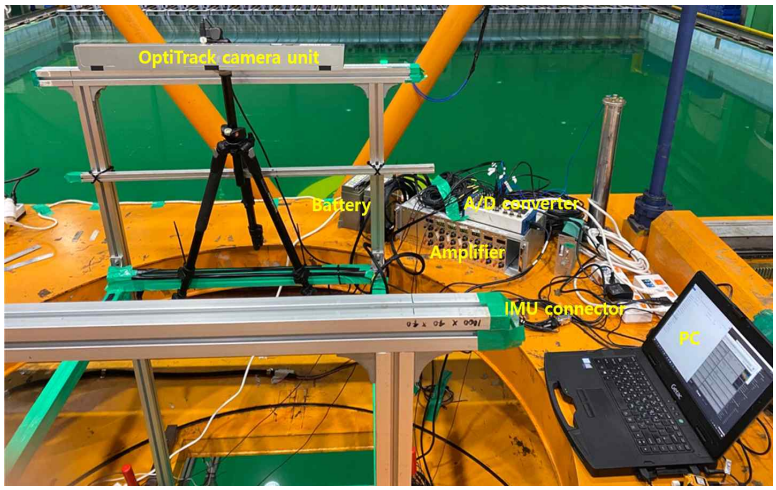

Fig. 4.25 Setup of data acquisition of measurement sensor

4.5.3. Data acquisition

In the table 4.12 are listed the value data which are measured from the sensors by OptiTrack, IMU, Tension gauge.

Table 4.12 Data acquired by the sensors

Sensor	Data type
Wave probe	ζ
OptiTrack	$x,\ y,\ z,\ \phi,\ \theta,\ \psi$
IMU	$\phi,\ \theta,\ \psi,$
Tension gauge	$T_1,\ T_2,\ T_3,\ T_4$

The data acquired by the wave probe, tension gauge are taken in the data acquisition system with 4 channels. The signal from IMU sensors was recorded in the MIP Monitor software and the signal from OptiTrack is given based on the recording the motion of the markers. As shows in fig. 4.13 the coordinate system of the OptiTrack.

Table 4.13 Definition of OptiTrack coordinate system

Seakeeping	OptiTrack
x_b	z_{OT}
y_b	x_{OT}
z_b	$-y_{OT}$

On the other hand, the signal of rotation angle from OptiTrack is the quaternions. Eq (4.4~4.6) to convert from quaternions to Euler angles. Fig. 4.26 the process for convert coordinate system of OptiTrack by python program.

- A unit quaternion,

$$e = [\varepsilon_1 \, \varepsilon_2 \, \varepsilon_3 \, \eta]^T \tag{4.4}$$

- This parameterization implies that the Euler parameters satisfy the constraint $e^T e = 1$,

$$\varepsilon_1^2 + \varepsilon_2^2 + \varepsilon_3^2 + 1 = 1 \tag{4.5}$$

- The transformation matrix is expressed as follows,

$$E_1(e) = \begin{bmatrix} 1-2(\varepsilon_2^2+\varepsilon_3^2) & 2(\varepsilon_1\varepsilon_2-\varepsilon_3\eta) & 2(\varepsilon_1\varepsilon_3+\varepsilon_2\eta) \\ 2(\varepsilon_1\varepsilon_2+\varepsilon_3\eta) & 1-2(\varepsilon_1^2+\varepsilon_3^2) & 2(\varepsilon_2\varepsilon_3-\varepsilon_1\eta) \\ 2(\varepsilon_1\varepsilon_3-\varepsilon_2\eta) & 2(\varepsilon_2\varepsilon_3+\varepsilon_1\eta) & 1-2(\varepsilon_1^2+\varepsilon_2^2) \end{bmatrix} \tag{4.6}$$

```python
def euler_from_quaternion(x, y, z, w):
        """
        Convert a quaternion into euler angles (roll, pitch, yaw)
        roll is rotation around x in radians (counterclockwise)
        pitch is rotation around y in radians (counterclockwise)
        yaw is rotation around z in radians (counterclockwise)
        """
        t0 = +2.0 * (w * x + y * z)
        t1 = +1.0 - 2.0 * (x * x + y * y)
        roll_x = math.atan2(t0, t1)

        t2 = +2.0 * (w * y - z * x)
        t2 = +1.0 if t2 > +1.0 else t2
        t2 = -1.0 if t2 < -1.0 else t2
        pitch_y = math.asin(t2)

        t3 = +2.0 * (w * z + x * y)
        t4 = +1.0 - 2.0 * (y * y + z * z)
        yaw_z = math.atan2(t3, t4)

        return roll_x, pitch_y, yaw_z # in radians
```

Fig. 4.26 Convert coordinate system of OptiTrack by python program

4.6. Roll decay test

Fig. 4.27~4.29 show the time series of ship decay tests for heave, roll, pitch, respectively. The ship decay test were performed with soft mooring system (mooring lines, springs, tension gauges) and three times at zero speed. Because the mooring system affects the vertical motion, the periods of heave and pitch are slightly slower. However, the period of roll motion is not affects by mooring systems. Table 4.14 the results of mean three times were measured of ship decay test for rotational motion.

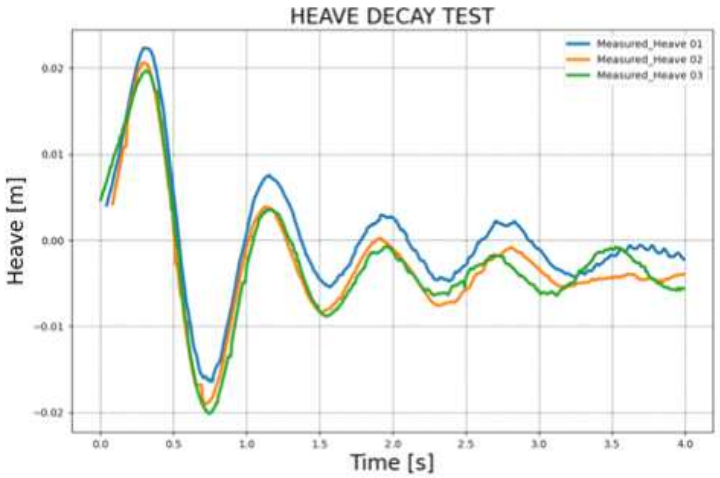

Fig. 4.27 Time series of heave decay test

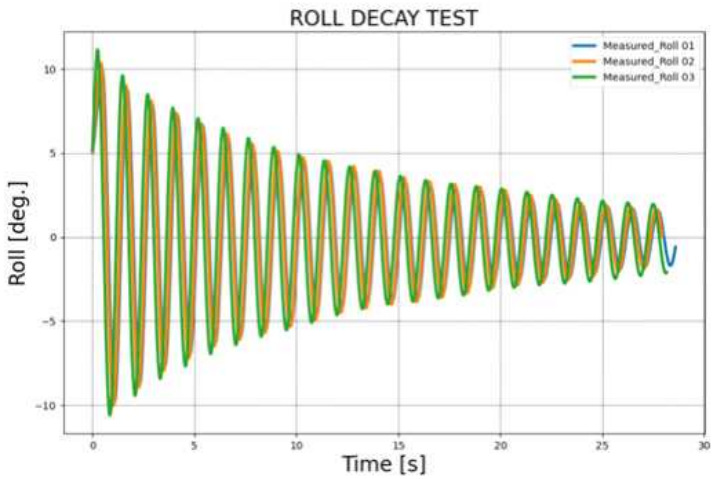

Fig. 4.28 Time series of roll decay test

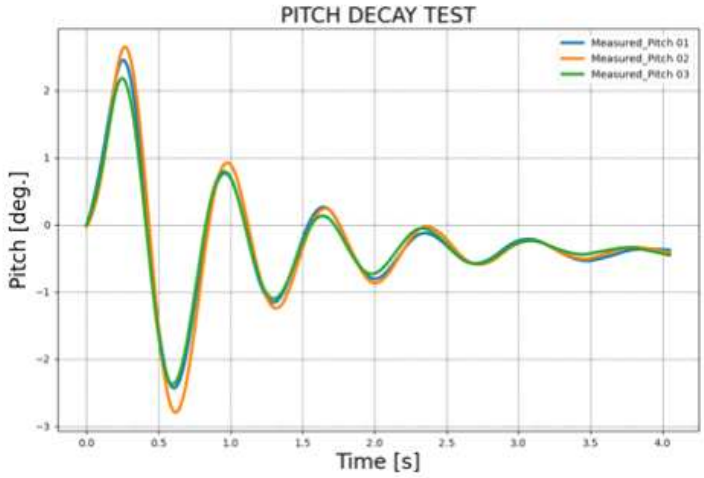

Fig. 4.29 Time series of pitch decay test

Table 4.13 Results measured mean of three times decay test

No	Roll_deg./s	Pitch_deg./s	Heave_m/s
01	1.240	0.695	0.825
02	1.245	0.695	0.125
03	1.240	0.700	0.821
Mean	1.240	0.695	0.820

5. Result and discussion

5.1. Data analysis

The seakeeping performance in regular waves were conducted in the 3D wave tank in Changwon National University to measure the wave force acting on the model KVLCC2 ship with 6-DOF motion. The seakeeping test for model ship were performed for 5 wave directions at zero speed. The motions in regular waves were analyzed using Fourier analysis. The Fourier coefficients for harmonic motion can be obtained through the least squares method. Fig 5.1 shows the examples of the results of frequency fitting of time series for motion measured by OptiTrack for different conditions.

- The definition of harmonic motion is expressed as Eq. (5.1),

$$z(t) = a_0 + a_1\cos(\omega t) + a_2\sin(\omega t) \tag{5.1}$$

- Fourier coefficients are calculated as Eq. (5.2),

$$\underline{\beta} = \begin{bmatrix} a_1 & a_2 & a_3 \end{bmatrix}^T \tag{5.2}$$

- Fourier coefficient vector can be obtained as Eq. (5.3),

$$\underline{\beta} = (H^T H)^{-1} H^T \underline{Z} \tag{5.3}$$

$$H = \begin{bmatrix} 1 & \cos\omega t_1 & \sin\omega t_1 \\ 1 & \cos\omega t_2 & \sin\omega t_2 \\ \vdots & \vdots & \vdots \\ 1 & \cos\omega t_n & \sin\omega t_n \end{bmatrix} \tag{5.4}$$

$$\underline{Z} = \begin{bmatrix} z(t_1) & z(t_2) & \cdots & z(t_n) \end{bmatrix}^T \tag{5.5}$$

- On the other hand, wave force is analyzed using Fourier analysis in the form of a fourth harmonic function as Eq. (5.6),

$$\begin{aligned} f(t) = f_0 &+ f_1\cos(\omega_e t + \varepsilon_1) + f_2\cos(2\omega_e t + \varepsilon_2) \\ &+ f_3\cos(3\omega_e t + \varepsilon_3) + f_4\cos(4\omega_e t + \varepsilon_4) \end{aligned} \tag{5.6}$$

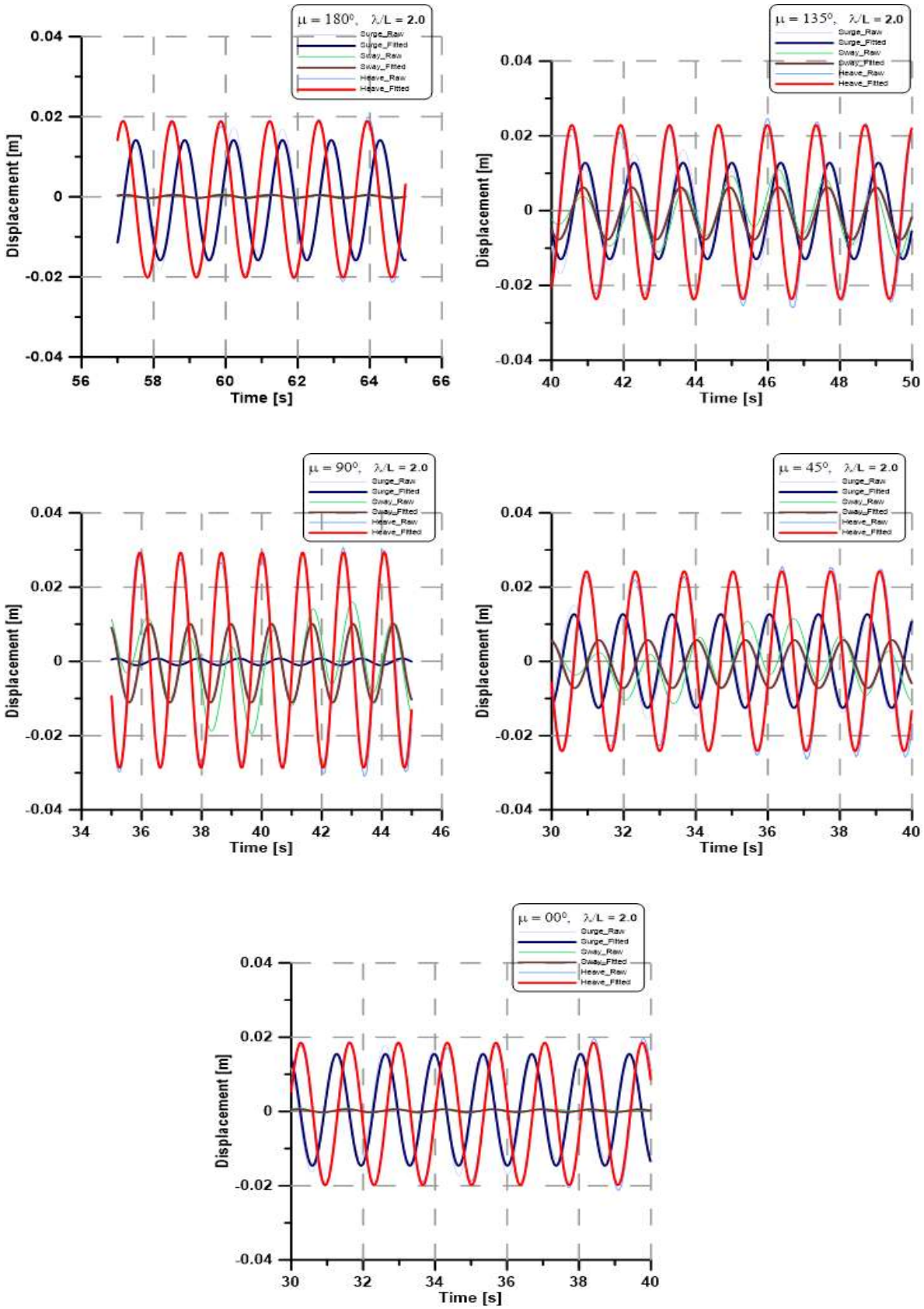

Fig. 5.1 Time series of motion measured by OptiTrack with $\omega = 4.634$ rad/s

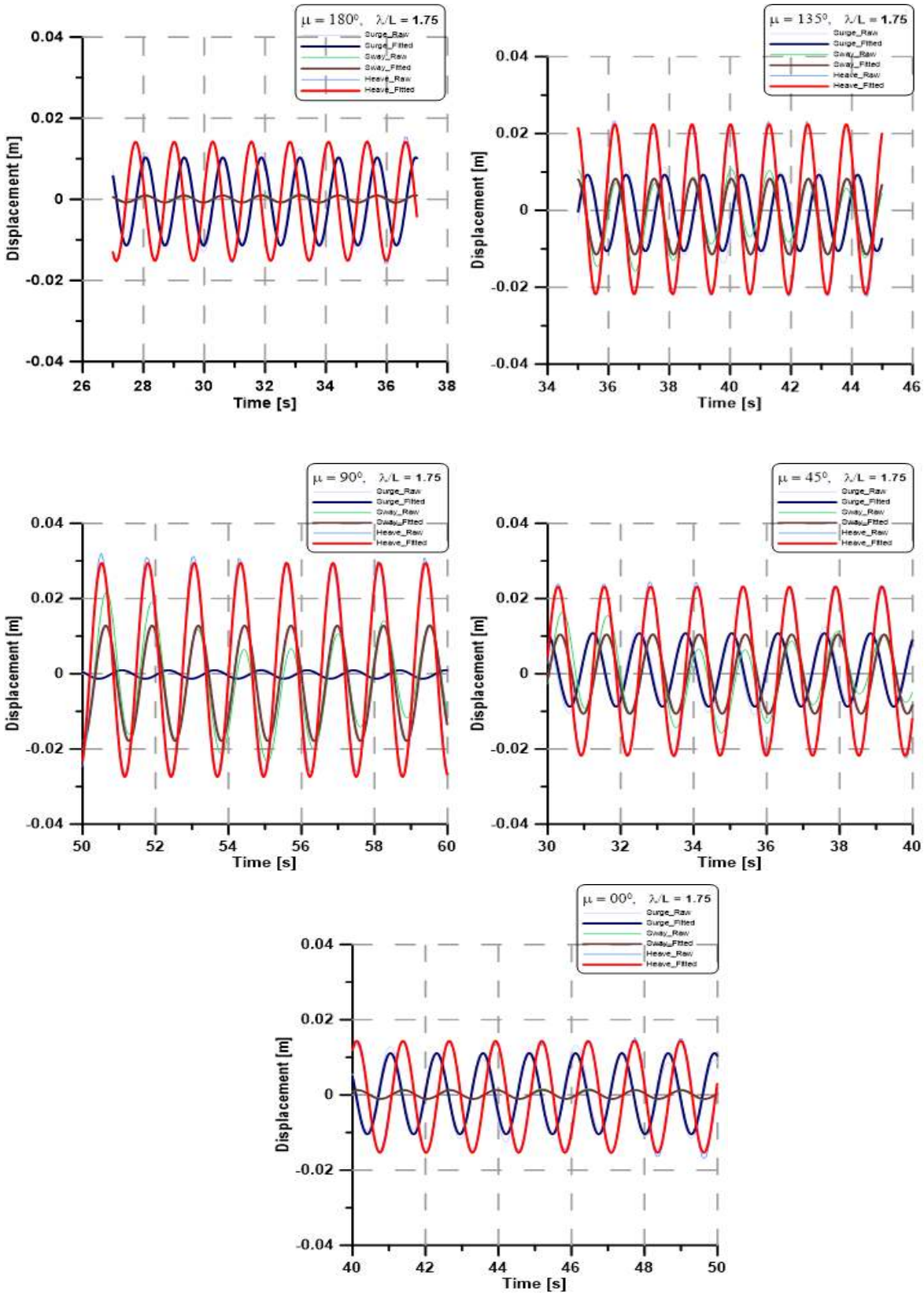

Fig. 5.2 Time series of motion measured by OptiTrack with $\omega = 4.954$ rad/s

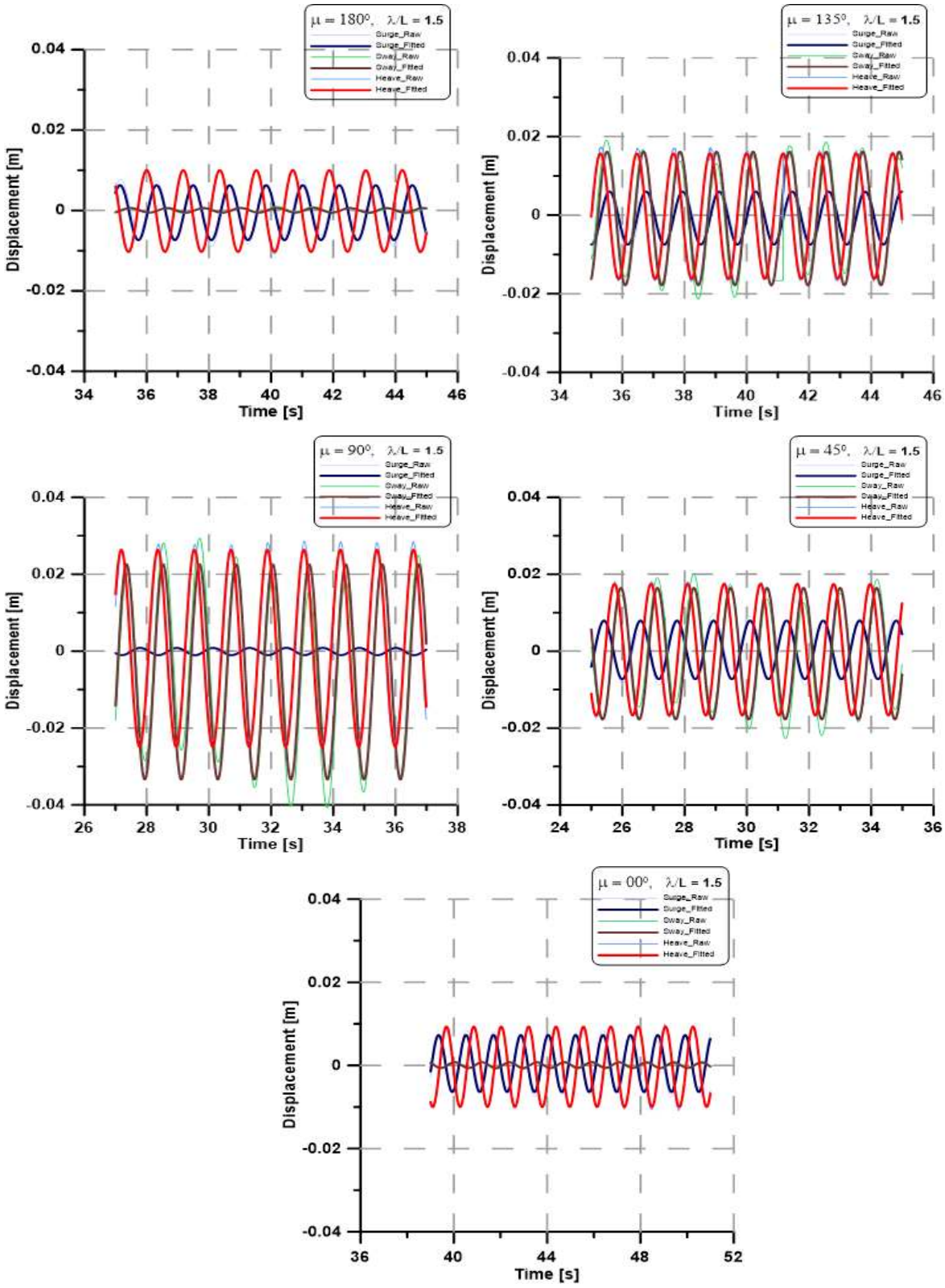

Fig. 5.3 Time series of motion measured by OptiTrack with $\omega = 5.351$ rad/s

5.2. Comparison of motion response in regular waves

The wave drift forces acting on a ship are dominantly affected by the ship's motion responses and the surrounding wave fields, because of that the motion responses of the ship must be predicted with high accuracy. In this section, the motion RAOs of KVLCC2 in regular waves are investigated in various wave directions with the range of λ/L form 0.5 to 2.0 are first checked. In addition, model ship motion is measured using OptiTrack and IMU in regular waves. The displacements of the motion are analyzed by Fourier analysis and motion RAOs was calculated by Eqs. (5.7~5.8) for translational and rotational motion, respectively. The x-axis represented the wavelength divided by the ship length, whereas the y-axis represented the motion RAOs normalized by the wave amplitude. Fig. 5.4 show the surge, sway, heave, roll, pitch, and yaw motion RAOs of KVLCC2 under head sea conditions 180 degrees. In the same cases for 90 degrees and 0 degrees of Fig. (5.5~5.6), respectively. In the figures, the results of two different betweens simulation and experiment are presented together for comparison. Comparing the model test data with the numerical calculations by AWQUA software showed good agreement in the overall tendencies and magnitudes. The motion characteristics of the ship altered according to the different wave direction as well as range of λ/L. Nevertheless, a few points (for example, roll RAO, 90 degrees) did not well. The non-dimensional translation and rotation responses can be determined as:

$$\text{For translations: } RAO = \frac{x, y, z}{\zeta_a} \tag{5.7}$$

$$\text{For rotations: } RAO = \frac{\phi, \theta, \psi}{k\zeta_a} \tag{5.8}$$

Here, ζ_a is the wave amplitude and k is the wave number.

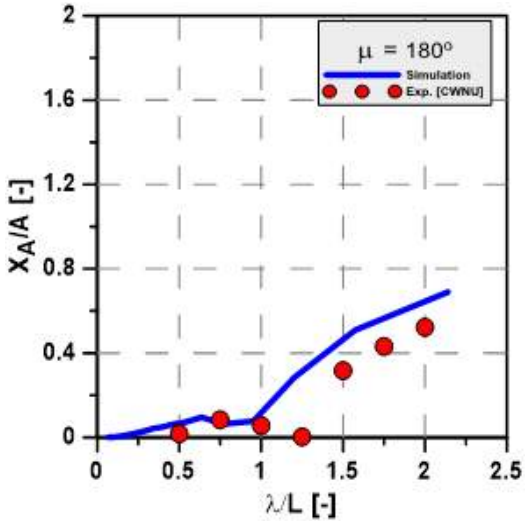

a) Surge motion RAO

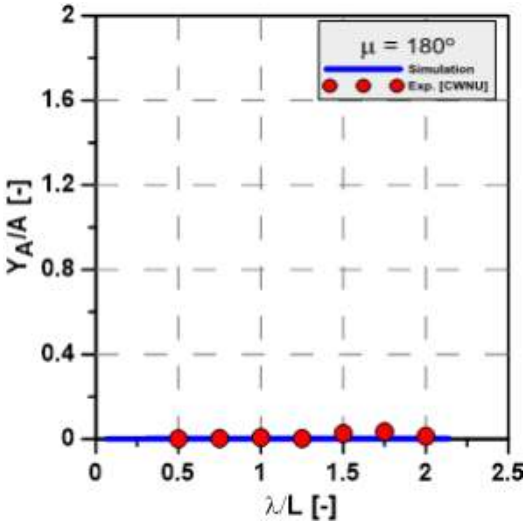

b) Sway motion RAO

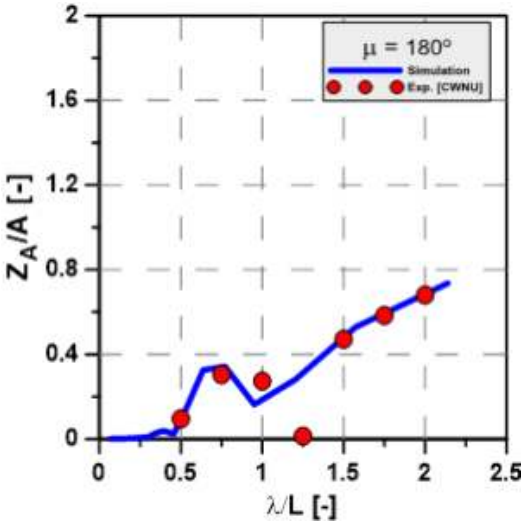

c) Heave motion RAO

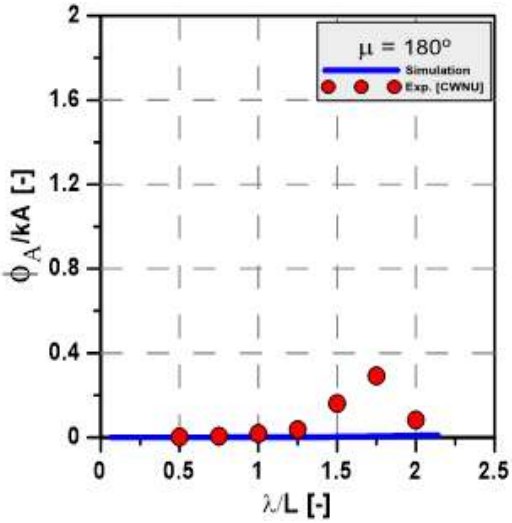

d) Roll motion RAO

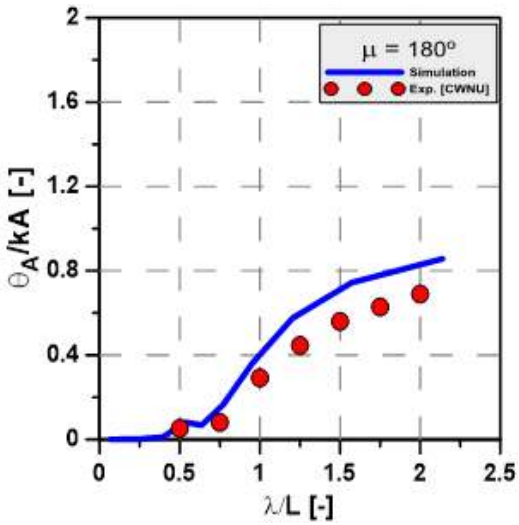

d) Pitch motion RAO

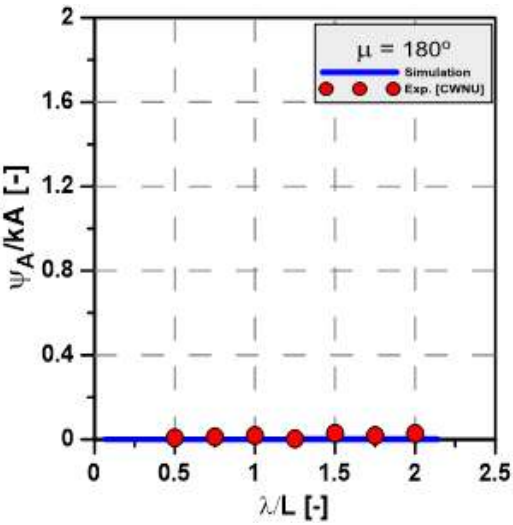

e) Yaw motion RAO

Fig 5.4 Motion response amplitude operators (RAOs): $\mu = 180$ deg

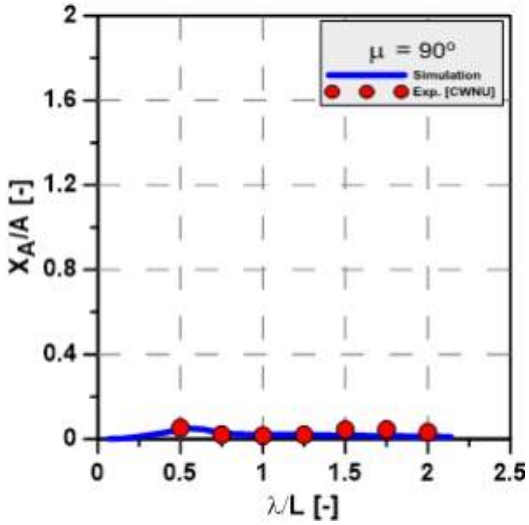

a) Surge motion RAO

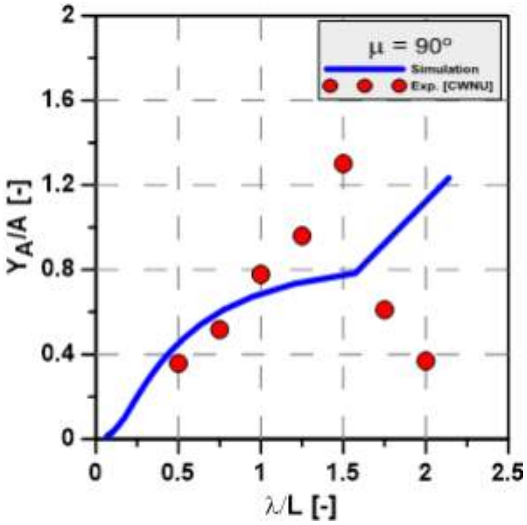

b) Sway motion RAO

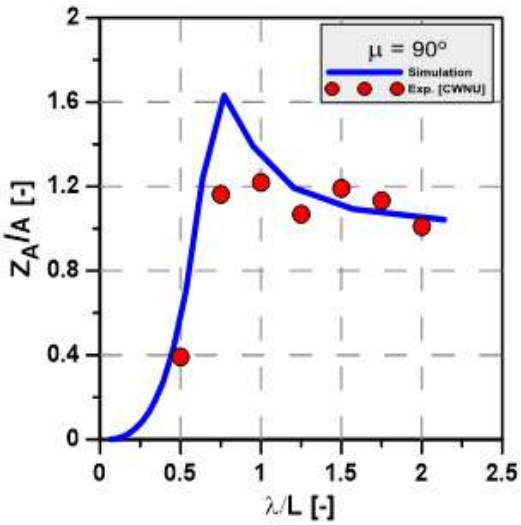

c) Heave motion RAO

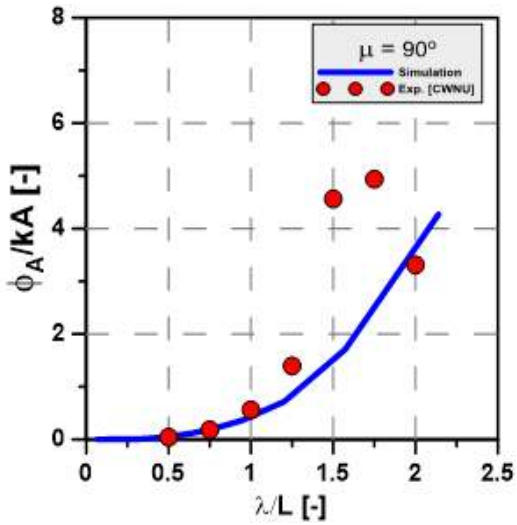

d) Roll motion RAO

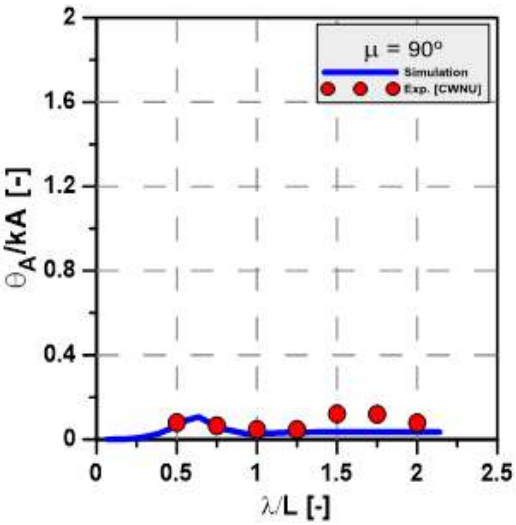

d) Pitch motion RAO

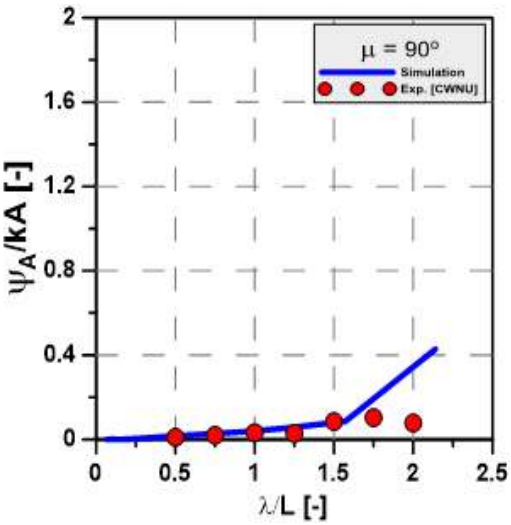

e) Yaw motion RAO

Fig. 5.5 Motion response amplitude operators (RAOs): $\mu = 90$ deg

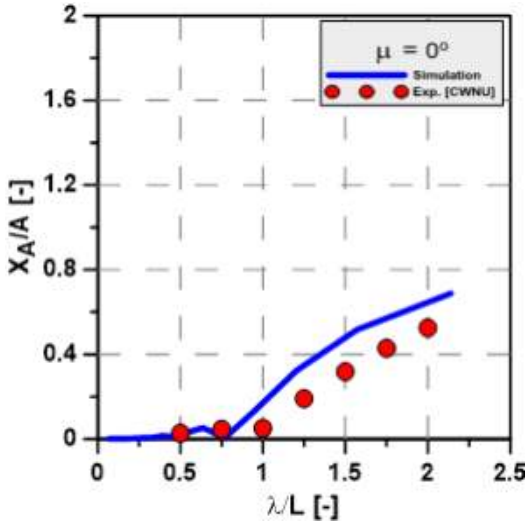

a) Surge motion RAO

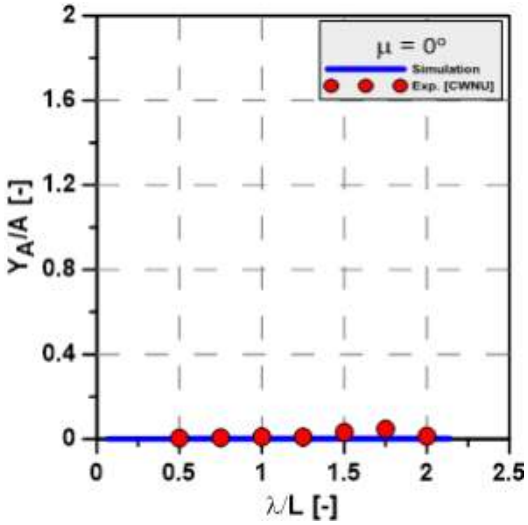

b) Sway motion RAO

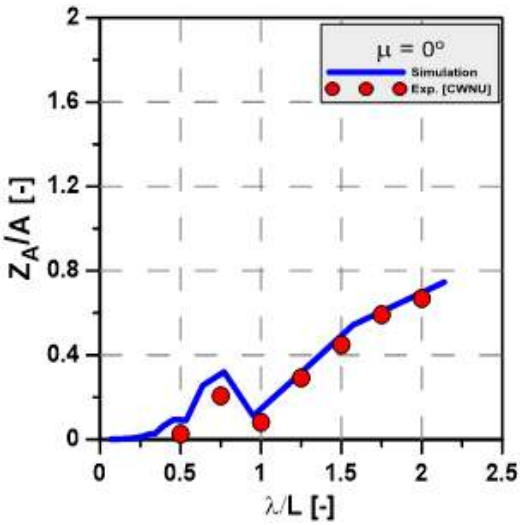

c) Heave motion RAO

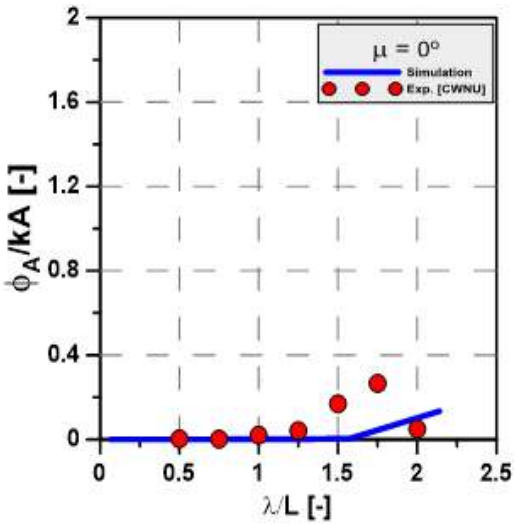

d) Roll motion RAO

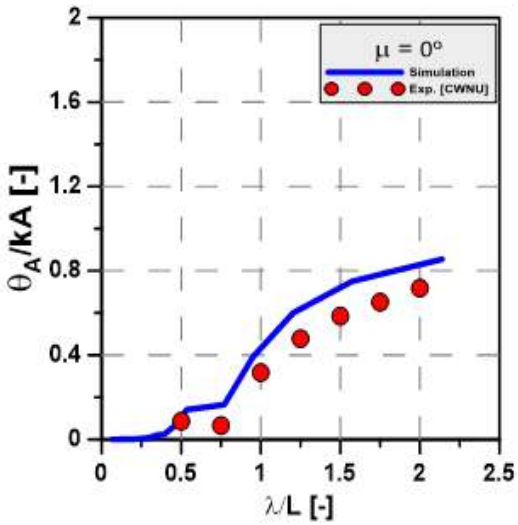

d) Pitch motion RAO

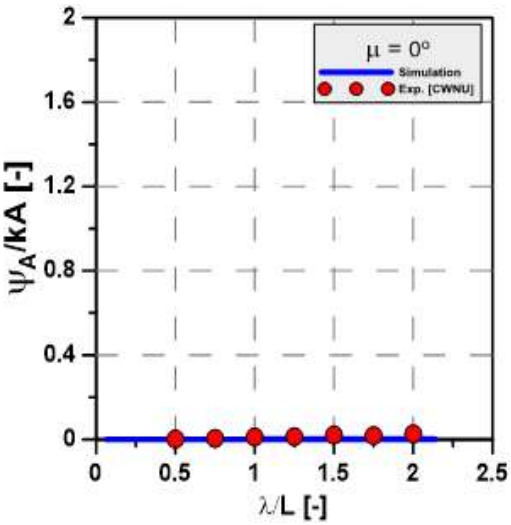

e) Yaw motion RAO

Fig. 5.6 Motion response amplitude operators (RAOs): $\mu = 0$ deg

5.3. Comparison of wave drift force

In this section, wave drift force was measured using four tension gauges located at four mooring line angles connecting with springs and supported structure. The surge force, sway force and yaw moment of the model ship in waves are calculated by Eqs. (5.9) and Eq. (5.10) express the non-dimensional wave drift force acting on the ship. Fig. 5.7 The model ship schematic plan Fig. 5.8 shows the surge, sway and yaw moment of wave drift force results when KVLCC2 was at zero speed and different wave directions. The red square denotes the result measured from the experiment using the tension gauges. The x- and y-axes show the values of the non-dimensional wavelength and wave drift forces, respectively. A comparison of the present numerical results with the experimental data at head sea ($\mu = 90$ deg.) showed that the overall tendencies were similar to each other. With the case of surge drift force became the largest at the wavelength ratio around 0.5.

- Calculation of wave drift force,

$$\overline{X}_w = T_1\cos\alpha_1 + T_2\cos\alpha_2 - T_3\cos\alpha_3 - T_4\cos\alpha_4 \tag{5.9}$$

$$\overline{Y}_w = T_1\sin\alpha_1 - T_2\sin\alpha_2 - T_3\sin\alpha_3 + T_4\sin\alpha_4$$

$$\overline{N}_w = x_{Tf}(T_1\sin\alpha_1 - T_2\sin\alpha_2) + x_{Ta}(-T_3\sin\alpha_3 + T_4\sin\alpha_4)$$

Non-dimensional wave drift force,

$$\begin{cases} C_x = \dfrac{X_w}{\rho g h_a^2 B^2/L} \\ C_y = \dfrac{Y_w}{\rho g h_a^2 B^2/L} \\ C_n = \dfrac{N_w}{\rho g h_a^2 B^2} \end{cases} \tag{5.10}$$

Where,

T_1, T_2, T_3, T_4 : the force of tension gauges 1, 2, 3, 4, respectively

x_{Tf}, x_{Ta} : the displacement form bow and stern to center of ship

h_a : weight amplitude

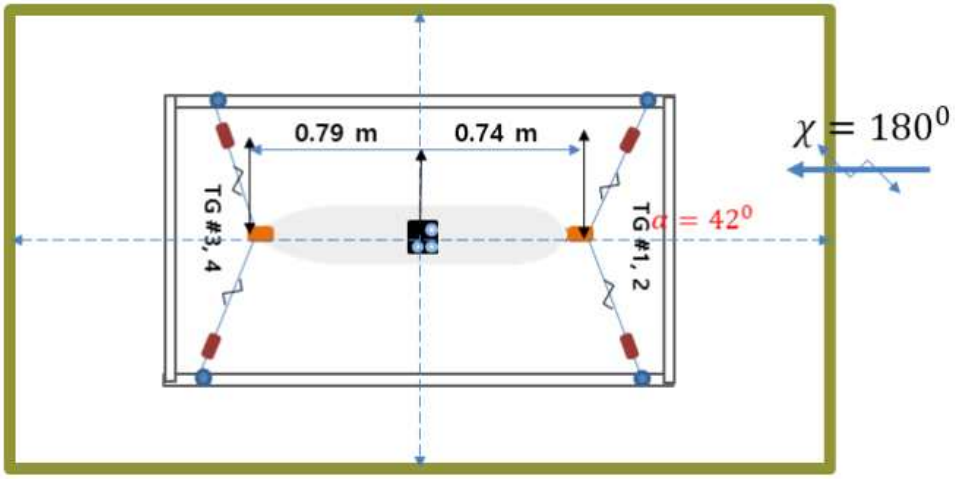

Fig. 5.7 The model ship schematic plan

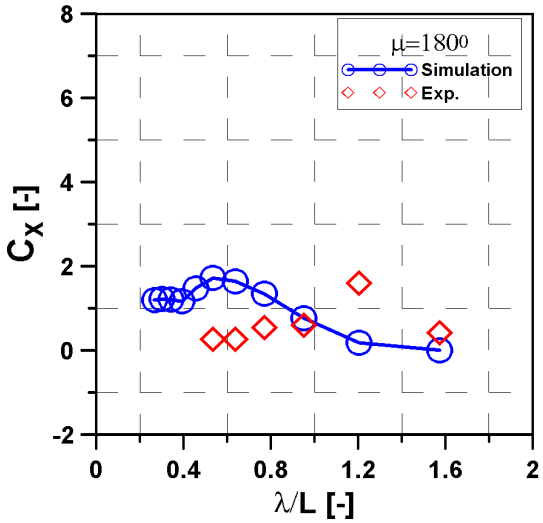

a) Surge wave drift force $\mu = 180$ deg.

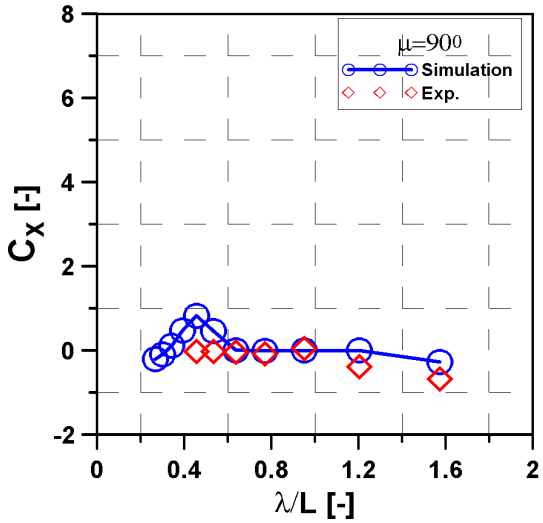

b) Surge wave drift force $\mu = 90$ deg.

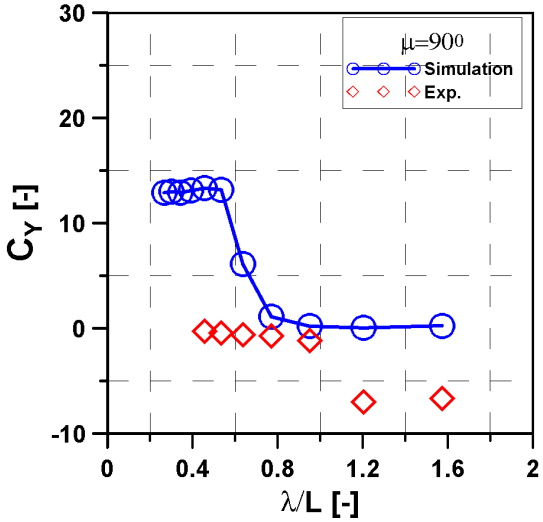

c) Sway wave drift force $\mu = 90$ deg.

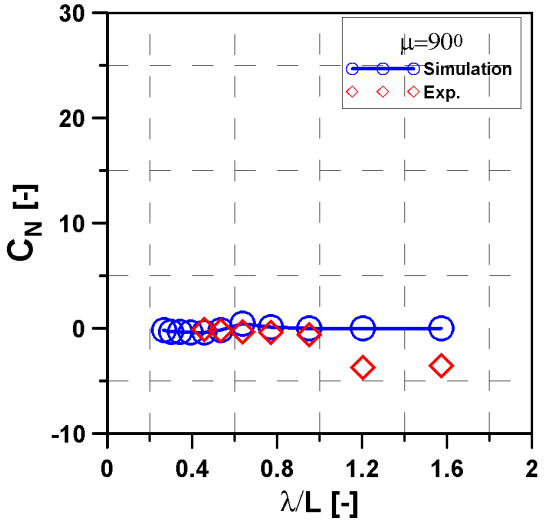

d) Yaw wave drift force $\mu = 90$ deg.

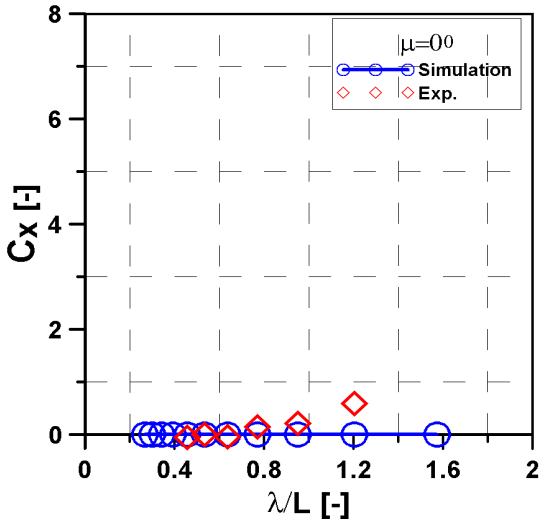

e) Surge wave drift force $\mu = 0$ deg.

Fig. 5.8 Results of wave drift force with different wave directions.

5.4. Conclusions

In this study, the wave drift force and moment as well as motion RAOs for KVLCC2 ship with forward speed were estimated using experiment ans numerical computation. A seakeeping test applying a soft spring-type mooring system was employed to control the horizontal motions was carried out in towing tank at Changwon National University under various wave conditions. Numerical analysis was performed using the AQWA program based on potential flow. Based on the current study, the following conclusions can be obtained:

- A measurement system for the wave drift force on a ship journey with forward speed and various wave directions was successfully investigated and developed. Adirect experiment method using force sensors is suitable for accurate measurement of the wave drift force and moment;
- Through a experiment of model tests, the validation data for the wave drift force was obtained. It was compared as well as confirmed that overall tendency of the wave drift force and moment calculated using the numerical method was similar to experimental data;
- In the case of the surge drift force measured by the experimental method, the overall trends were similar, but the magnitude near the short wavelength less than 0.8 was smaller than the experimental value.

3. 연구결과 활용방안

○ Application in other Marine engineering field

- Evaluate the ship or offshore plant's performance in waves
- Suggest SW or class of 2nd-order drift force model to SW engineers to develop HIL test of marine systems.

4. 기대효과

○ Accurate estimation of 2nd-order wave drift force

- Propose the 2nd-order wave drift force model to simulate dynamic positioning of offshore plant or an offloading shuttle tanker to confirm those performance before construction, which will reduce lots of design mistakes.
- Store valuable experimental results which will be used to confirm the theoretical results of the other researchers.

참고문헌

1. Wei Zhang; Ould el Moctar; Thomas E.Schellin. Numerical study on wave-induced motions and steady wave drift forces for ships in oblique waves.
2. Min Guk Seo; Yoon Jin Ha; Bo Woo Nam; Yeongyu Kim. Experimental and numerical analysis of wave drift force on KVLCC2 moving in oblique waves.
3. Zhang, S.; Weems, K.M.; Lin, W.-M. Investigation of the horizontal drifting effects on ships with forward speed. In Proceedings of the 28th International Conference on Ocean, Offshore and Arctic Engineering, Honolulu, HI, USA.